JCB Journal of Cell Biology

ARTICLE

BRG1 programs PRC2-complex repression and controls oligodendrocyte differentiation and remyelination

Jiajia Wang[1,2], Lijun Yang[1], Yiwen Du[2], Jincheng Wang[1], Qinjie Weng[2], Xuezhao Liu[1], Eva Nicholson[1], Mei Xin[1], and Qing Richard Lu[1,3]

Chromatin-remodeling protein BRG1/SMARCA4 is pivotal for establishing oligodendrocyte (OL) lineage identity. However, its functions for oligodendrocyte-precursor cell (OPC) differentiation within the postnatal brain and during remyelination remain elusive. Here, we demonstrate that *Brg1* loss profoundly impairs OPC differentiation in the brain with a comparatively lesser effect in the spinal cord. Moreover, BRG1 is critical for OPC remyelination after injury. Integrative transcriptomic/genomic profiling reveals that BRG1 exhibits a dual role by promoting OPC differentiation networks while repressing OL-inhibitory cues and proneuronal programs. Furthermore, we find that BRG1 interacts with EED/PRC2 polycomb-repressive-complexes to enhance H3K27me3-mediated repression at gene loci associated with OL-differentiation inhibition and neurogenesis. Notably, BRG1 depletion decreases H3K27me3 deposition, leading to the upregulation of BMP/WNT signaling and proneurogenic genes, which suppresses OL programs. Thus, our findings reveal a hitherto unexplored spatiotemporal-specific role of BRG1 for OPC differentiation in the developing CNS and underscore a new insight into BRG1/PRC2-mediated epigenetic regulation that promotes and safeguards OL lineage commitment and differentiation.

Introduction

Oligodendrocytes (OLs) are specialized cells of the central nervous system (CNS) that form myelin sheaths to ensure proper electrical impulse conduction along their axons (Bercury and Macklin, 2015). OL development is a sequential process that begins with lineage specification of neural progenitor cells into primitive early oligodendrocyte progenitor cells (e.g., pri-OPC or pre-OPC) (Weng et al., 2019) marked by lineage transcription factors Olig1/2, followed by their lineage commitment as OPCs (PDGFRα$^+$ or NG2$^+$) (Nishiyama et al., 2021). These OPCs then undergo differentiation into pre-myelinating OLs before eventually maturing into myelinating OLs that are capable of forming myelin sheaths (Berry and Lu, 2020; Nishiyama et al., 2021; Weng et al., 2019). This step-wise differentiation process requires coordination of extracellular and intracellular regulators, including stage-specific transcriptional regulators as well as epigenetic or chromatin modifiers that alter the chromatin state to control gene transcription (Emery and Lu, 2015; Sun et al., 2018; Wegner, 2008; Zuchero and Barres, 2013). Failure of remyelination by surviving or newly generated OLs after injury or other pathological insults can cause disruptions in axonal transmission, leading to deficits in motor and cognitive functions, or demyelinating diseases such as multiple sclerosis and leukodystrophy (Franklin and Goldman, 2015; McKenzie et al., 2014).

Chromatin modification and remodeling are critical molecular processes that underpin OL lineage differentiation (Emery and Lu, 2015; Koreman et al., 2018). ATP-dependent chromatin remodelers use ATP to unwind, slide, and/or displace individual nucleosomes and gate the accessibility of chromatin to lineage-specific transcriptional regulators for target gene expression (Hota and Bruneau, 2016; Runge et al., 2016). Notably, members of the SWI/SNF family of chromatin remodelers carry out such molecular functions to regulate cell growth, differentiation, and regeneration (Hargreaves and Crabtree, 2011; Ho and Crabtree, 2010). Brahma-related 1 (BRG1; also known as SMARCA4) is the central ATPase catalytic subunit of the SWI/SNF chromatin remodeling complex (Centore et al., 2020). BRG1 contains a bromodomain that recognizes acetylated lysines on histone tails, facilitating the targeting of the SWI/SNF complex to active enhancer/promoter elements, which enhances RNA Polymerase II occupancy, thereby activating gene transcription (Centore et al., 2020; Tolstorukov et al., 2013; Yu et al., 2013).

[1]Division of Experimental Hematology and Cancer Biology, Cincinnati Children's Hospital Medical Center, Cincinnati, OH, USA; [2]Center for Drug Safety Evaluation and Research, College of Pharmaceutical Sciences, Zhejiang University, Hangzhou, China; [3]Division of Developmental Biology, Department of Pediatrics, University of Cincinnati School of Medicine, Cincinnati, OH, USA.

Correspondence to Qing Richard Lu: richard.lu@cchmc.org.

BRG1 chromatin-remodeling complex can be recruited by the OL lineage specification factor Olig2 to target OL-specific enhancers (Yu et al., 2013). Functional cooperation between BRG1-dependent chromatin-remodelers with Olig2 is vital for initiating and establishing the transcriptional program necessary for OL differentiation (Yu et al., 2013). Consistently, neural progenitor cells (NPCs) lacking *Brg1* fail to differentiate into OPCs in the early embryonic cortex, even with ectopic upregulation of Olig2 in these cells (Matsumoto et al., 2016). The deletion of *Brg1* in *Olig1*+ lineage cells, initiating at the pre-OPC stage before the transition to committed OPCs, results in profound defects in OL differentiation and subsequent myelination (Yu et al., 2013). However, the role of BRG1 in differentiation onward from the committed OPC stage in the postnatal developing brain has not been defined. Since the OL progenitor pools are heterogeneous and distinct across the brain and spinal cord (Kessaris et al., 2006; Khandker et al., 2022; Weng et al., 2019; Yue et al., 2006), the roles of BRG1 in mediating the developmental progression of OPCs and myelinogenesis in a region- and stage-specific manner are not fully understood. A previous study found that conditional loss of *Brg1* in OLs directed by a *Cnp-Cre* driver, which predominantly drives gene loss in postmitotic and differentiating OLs, results in a moderate defect in OL differentiation within the developing spinal cord (Bischof et al., 2015). However, at present, the roles of BRG1 in the process of OPC differentiation into mature OLs in the developing brain remain elusive. Additionally, whether BRG1 is critical for OL remyelination after demyelinating injury is not known. Gaining insights into the functions of BRG1 during development and repair is critical for better understanding its role in disorders, including Coffin–Siris syndrome (CSS), which is characterized by white matter defects (Li et al., 2020; Tsurusaki et al., 2012), and related conditions collectively referred to as Coffin–Siris and BRG1- or HRBM-associated factor related (CSS-BAF) disorders (Vasko et al., 2021; Zarate et al., 2016).

In this study, by generating a stage-specific knockout mouse model with *Brg1* ablation in the PDGFRα⁺ OPC population, we find that BRG1 is important for OPC differentiation in the developing brain and, to a lesser extent, in the developing spinal cord at the postnatal stage. Furthermore, the remyelination following LPC injury is impeded by the loss of BRG1 function in PDGFRα⁺ OPCs. Integrated transcriptome and genomic profiling analysis indicate that BRG1 plays a dual role in facilitating the differentiation of OPC lineage while suppressing inhibitory pathways for OL lineage differentiation such as WNT and BMP signaling. The loss of *Brg1* also disrupts the repression of neuronal differentiation by the polycomb repressive–complex PRC2, leading to an upregulation of neurogenic genes. Furthermore, we find that BRG1 interacts with the EED/PRC2 complex to promote PRC2-mediated H3K27me3 suppression of genes associated with OL differentiation inhibition and neuronal differentiation. Together, our findings demonstrate that BRG1 has distinct stage- and region-specific roles in OL differentiation between the developing brain and spinal cord, as well as a pivotal role in myelin repair. Our study further provides an unprecedented insight into BRG1-PRC2-mediated epigenetic programming that facilitates and maintains OL lineage progression while suppressing the alternative neuronal lineage programs.

Results

Brg1 ablation in PDGFRα⁺ OPCs at the postnatal stages leads to OL differentiation defects in the developing brain

To investigate the function of BRG1 in differentiation and myelination of OPCs during postnatal brain development, we generated conditional *Brg1* mutants with *Brg1* ablation in PDGFRα⁺ OPCs by crossing $Brg1^{flox/flox}$ mice with tamoxifen-inducible *Pdgfra-CreERT* transgenic mice carrying a Rosa26-tdTomato reporter. Tamoxifen was administrated in control (*Pdgfra-CreERT*; $Brg1^{flox/+}$ or *Pdgfra-CreERT*) and *Brg1* iKO-*Pdgfra* (*Pdgfra-CreERT*; $Brg1^{flox/flox}$) mice from postnatal day 1 (P1) to P3, when most of the OL lineage cells are at the OPC stage (Fig. 1 A). Immunostaining confirmed that BRG1 was effectively deleted in the tdTomato⁺ reporter cells within the brains of *Brg1* iKO-*Pdgfra* mice (Fig. 1 B), while OLIG2 expression was still detected *n Brg1*-deficient OPCs (Fig. 1 C), suggesting that *Brg1* deletion in OPCs did not alter Olig2 expression substantially. A significant decrease in mature OLs marked by CC1 was observed in the white matter of *Brg1* iKO-*Pdgfra* mice at P14 when compared with control littermates (Fig. 1 D). Also, fewer numbers of MBP⁺ tdTom⁺ cells were observed within the corpus callosum of iKO-*Pdgfra* mice at P7 (Fig. 1 E), and the percentage of MBP⁺ myelinating area of the cerebral white matter at P7 and P14 mice was also markedly reduced (Fig. 1, F and G). These findings indicate that *Brg1* ablation in the PDGFRα⁺ OPCs inhibits their differentiation and maturation in the developing postnatal brain.

BRG1 is not required for OPC proliferation and cell survival in the postnatal brain

Given the possibility that the dysmyelination phenotype in *Brg1* iKO-*Pdgfra* mice could be caused by a failure of OPC proliferation or cell death, we investigated OPC development in the *Brg1* iKO-*Pdgfra* brain. We performed immunolabelling for Ki67⁺ to mark proliferating OPCs and found that the proportion of proliferating OPCs (marked by their co-expression of PRGFRα) was not significantly different between control and *Brg1* iKO-*Pdgfra* mice (Fig. 1 H). In addition, we found no evidence of significant OPC death in *Brg1* iKO-*Pdgfra* brains compared with controls, as assayed by immunostaining for the apoptotic marker cleaved caspase 3 (CC3) (Fig. 1 I). Furthermore, *Brg1* ablation in PDGFRα⁺ OPCs did not significantly alter the proportions of microglia marked by Iba1 and astrocytes marked by GFAP (Fig. S1). Thus, these results suggest that *Brg1* ablation in PDGFRα⁺ cells did not significantly affect OPC survival and microglia and astrocyte populations within the postnatal brain.

Brg1 ablation in PDGFRα⁺ OPCs impairs myelinogenesis in the brain and spinal cord

In light of the downregulation of myelin proteins in the *Brg1*-ablated iKO-*Pdgfra* mice, we next examined myelin sheath assembly in brain and spinal cord tissues by electron microscopy. The ultrastructure analysis indicates that the percentage of myelinated axons in the corpus callosum was significantly

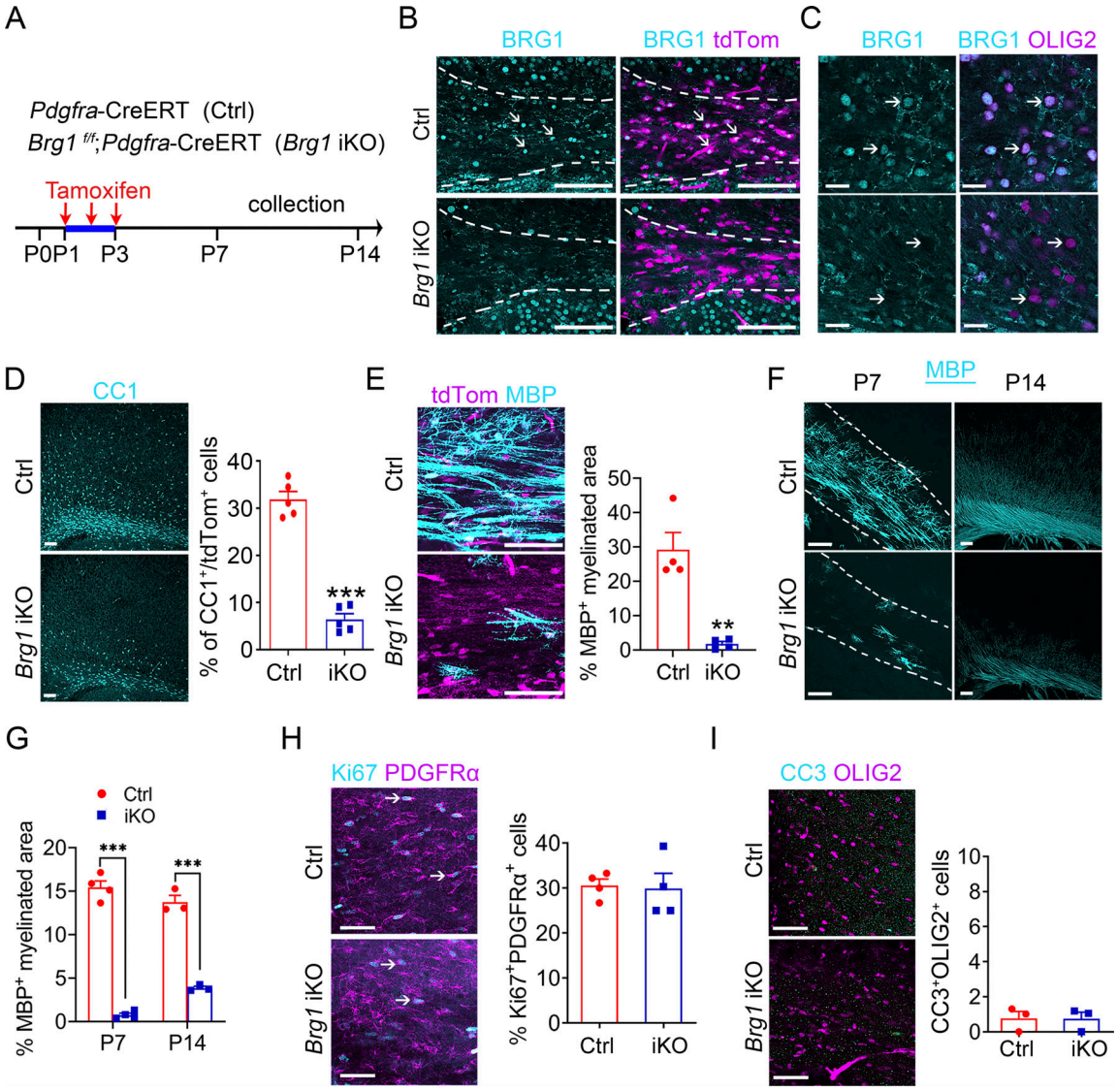

Figure 1. ***Brg1* deletion in PDGFRα⁺ OPC causes OL differentiation deficits in the brain. (A)** Strategy used to delete *Brg1* in postnatal OPCs by tamoxifen (TAM) administration. **(B)** Immunostaining for BRG1 antibody in the corpus callosum of control and *Brg1* iKO-*Pdgfra* mice at P7. Arrows indicate BRG1⁺/tdTomato⁺ cells. Scale bar, 50 µm; *n* = 4 animals/genotype. **(C)** Immunostaining for BRG1 and OLIG2 antibody in control and *Brg1* iKO-*Pdgfra* brains. Scale bar, 10 µm; *n* = 3 animals/genotype. **(D)** Immunostaining (left) and quantification (right) of CC1⁺/tdTomato⁺ cells in the corpus callosum of control and *Brg1* iKO-*Pdgfra* mice at P14. Scale bar, 50 µm; *n* = 5 animals/genotype. **(E)** Immunostaining of MBP in the white matter of control and *Brg1* iKO-*Pdgfra* mice at P7. Scale bar, 100 µm; *n* = 4 animals/genotype. **(F and G)** Immunostaining (F) and quantification (G) of MBP in the white matter of control and *Brg1* iKO-*Pdgfra* mice at P7 and P14. Scale bar in F, 50 µm. *n* = 4 animals/genotype at P7, *n* = 3 animals/genotype at P14. **(H)** Immunostaining (left) and quantification (right) of Ki67⁺/PDGFRα⁺ cells in the corpus callosum of control and *Brg1* iKO-*Pdgfra* mice at P7. Scale bar, 50 µm; *n* = 4 animals/genotype. **(I)** Immunostaining (left) and quantification (right) of cleaved-caspase 3⁺ (CC3⁺)/OLIG2⁺ cells in the corpus callosum of control and *Brg1* iKO-*Pdgfra* mice at P7. Scale bar, 50 µm; *n* = 3 animals/genotype. Data are presented as mean ± SEM; **P < 0.01; ***P < 0.001; two-tailed unpaired Student's *t* test (D, E, H, and I), two-way ANOVA with Sidak's multiple comparisons test (G).

reduced (57% in control compared with 15% in *Brg1* iKO-*Pdgfra* mice; P < 0.001) (Fig. 2, A and B).

To further investigate the region-specific function of BRG1 within the CNS, we examined the spinal cord and found that the proportion of myelinated axons in the spinal cord was decreased from 82% in the control to ∼40% in *Brg1* iKO-*Pdgfra* mice (Fig. 2, A and B). Deletion of BRG1 was confirmed in the spinal cords of *Brg1* iKO-*Pdgfra* mice, as marked by the expression of the reporter gene tdTom⁺ in cells that lacked BRG1 immunoreactivity (Fig. 2 C). We then quantified the number of tdTom⁺ cells that colabel with CC1 and found that the percentage of CC1⁺ mature OLs was significantly decreased in the spinal cord of P14 *Brg1* iKO-*Pdgfra* mice compared with the control (Fig. 2 D). Intriguingly, while we observed approximately threefold reductions in CC1-expressing cells and myelinated axons within the brains of iKO-*Pdgfra* mice compared with corresponding controls, the reductions of such cells and myelinated axons in the spinal cord of iKO-*Pdgfra* mice were less pronounced (twofold reductions or less). These observations suggest that BRG1 loss has a region-specific impact on OL myelination in the brain

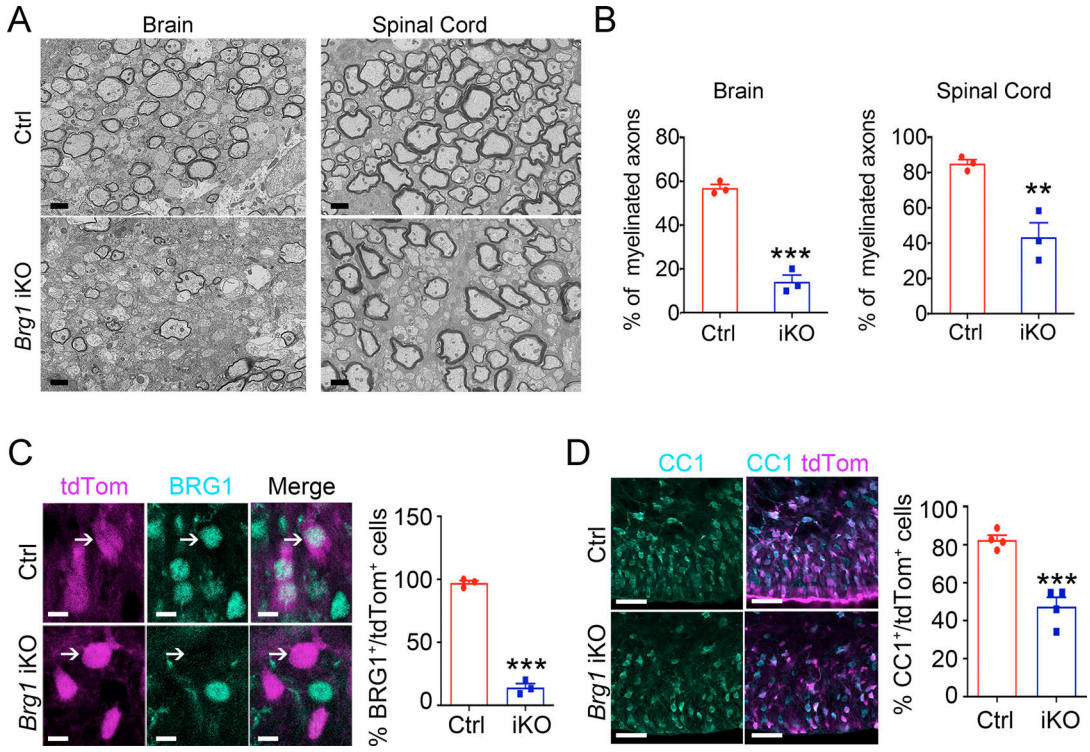

Figure 2. ***Brg1* iKO-*Pdgfra* mice develop myelinogenesis defects in the brain and spinal cord. (A)** Electron microscopy analysis of brain and spinal cord sections from P14 control and *Brg1* iKO-*Pdgfra* mice after TAM injections from P1 to P3. Scale bar, 2 mm; *n* = 3 animals/genotype. **(B)** Quantification of myelinated axons as a percentage of total axons from P14 control and *Brg1* iKO-*Pdgfra* brains and spinal cords. *n* = 3 animals/genotype. **(C)** Immunostaining (left) and quantification (right) of BRG1$^+$/tdTomato$^+$ cells in the ventral white matter of control and *Brg1* iKO-*Pdgfra* spinal cords at P14. Scale bar, 50 µm; *n* = 3 animals/genotype. **(D)** Immunostaining (left) and quantification (right) of CC1$^+$/tdTomato$^+$ cells in the white matter from P14 control and *Brg1* iKO-*Pdgfra* spinal cords. Scale bar, 100 µm; *n* = 4 animals/genotype. Data are presented as mean ± SEM; **P < 0.01; ***P < 0.001; two-tailed unpaired Student's *t* test (B–D).

and spinal cord, with varying severity between regions. Despite these regional differences in severity, the data indicate that BRG1 is necessary for PDGFRα$^+$ OPC differentiation and subsequent myelin formation during the development of the brain and spinal cord.

Brg1 deletion in *Cnp*$^+$ immature OLs at the embryonic stage causes a differentiation defect in the developing spinal cord

To investigate potential roles for BRG1 in the differentiation of immature OLs, we crossed *Brg1*$^{flox/flox}$ mice with a *CNP-Cre* line, in which the Cre recombinase transgene is expressed in immature differentiating OLs at the prenatal stage (Fig. S2 A). Immunostaining of these conditional knockout (cKO-*Cnp*) mice (*Cnp-Cre; Brg1*$^{flox/flox}$) showed that *Cnp*-Cre effectively depleted BRG1 in the cells of the white matter in the spinal cord at P1 (Fig. S2 B). We also performed in situ hybridization to find that expression levels for the myelin genes *Mbp* and *Plp1* were substantially diminished in the spinal cord of cKO-*Cnp* mice at E14.5 (Fig. S2, C and E). At P1, the number of mature OLs based on myelin gene expression *Mbp* and *Plp1* was also reduced in cKO-*Cnp* spinal cord, albeit to a lesser extent (Fig. S2, D and E), and this finding was consistent with previous observations (Bischof et al., 2015). Thus, our data indicate that the loss of BRG1 in the *Cnp*$^+$ immature OLs impairs OL differentiation in the embryonic spinal cord, but this phenotype is less pronounced at the early postnatal stage.

BRG1 is required for OL remyelination after injury in the spinal cord

Given its importance for OPC differentiation and OL myelination, we next investigated whether BRG1 is relevant to myelin regeneration, using an experimental model to induce demyelination in mice following exposure to l-α-Lysophosphatidylcholine (LPC). A single LPC injection induces a focal demyelinating lesion in the white matter of the spinal cord, which is accompanied by a spontaneous remyelinating process that is evident by 14 days post injection (dpi 14). As shown in Fig. 3, A and B, BRG1 expression at the site of injury was upregulated and detected in the majority of PDGFRα$^+$ OPCs within the lesion. To investigate the functional significance of BRG1 in remyelination, we treated control and *Brg1* iKO-*Pdgfra* mice with tamoxifen for 5 days before and 5 days after LPC injection into the ventral white matter to delete *Brg1* in PDGFRα$^+$ OPCs. The lesioned spinal cords were harvested and analyzed at dpi 14 and dpi 21 (Fig. 3 C). Our immunostaining data showed that the MBP immunofluorescence signal was reduced in the lesions of LPC-treated iKO-*Pdgfra* mice compared with controls at dpi 14 (Fig. 3 D). Also, we performed in situ hybridization (ISH) on samples from dpi 14 and dpi 21 and found that signals for *Mbp* and *Plp1* that label mature OLs were substantially decreased in the lesion of LPC-treated iKO-*Pdgfra* mice compared with control (Fig. 3, E–I). Consistent with an effect of BRG1-loss in OPCs on myelination, we examined the ultrastructural myelin sheaths

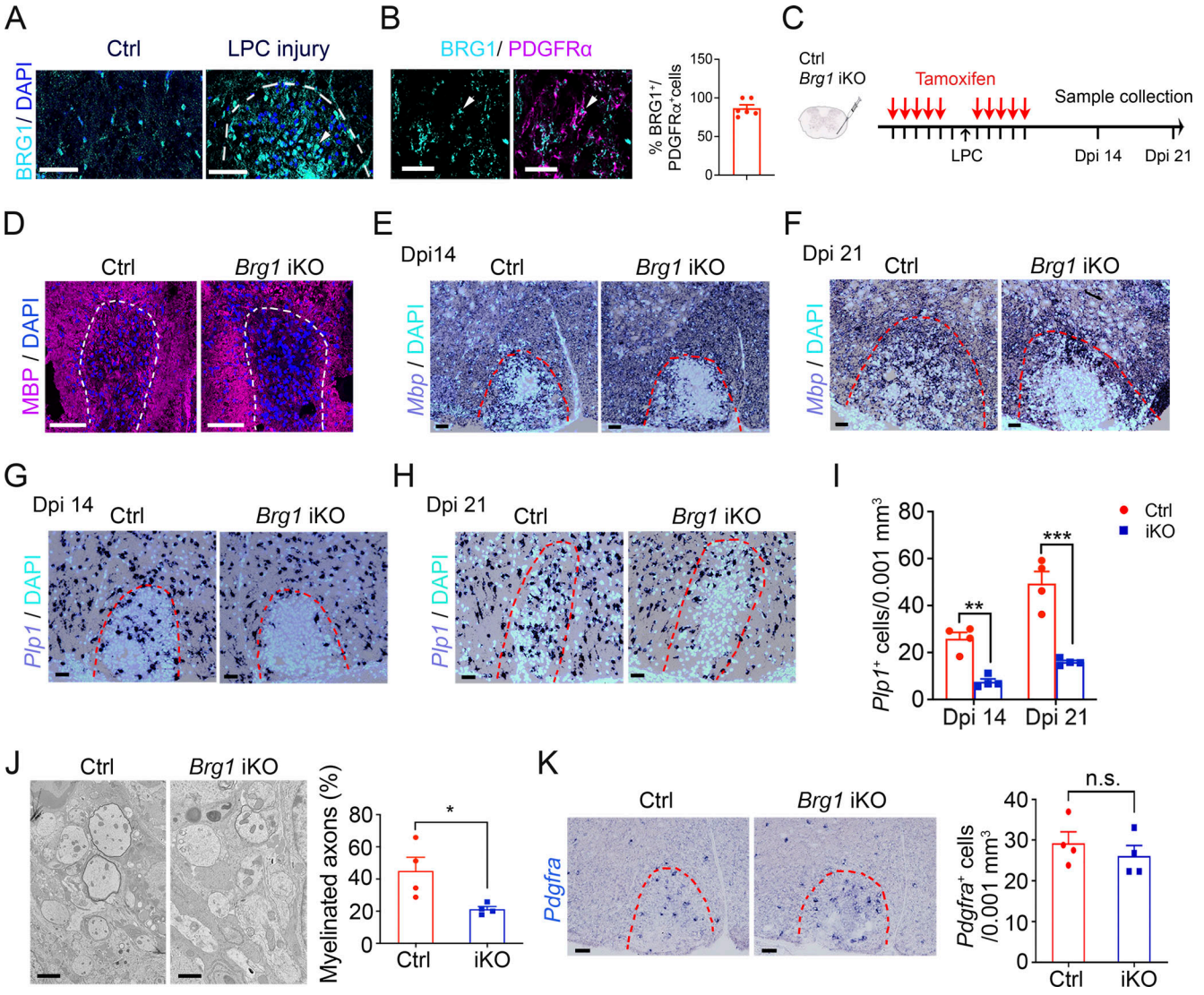

Figure 3. **BRG1 is critical for OPC remyelination after injury. (A)** Representative immunostaining of BRG1 at control and lesion sites after LPC injury at P7. Scale bar, 50 µm; *n* = 4 animals/group. Arrows, BRG1⁺ cells. **(B)** Representative immunostaining (left) and quantification (right) of BRG1⁺PDGFRα⁺ cells at LPC-lesion sites at dpi 7. Scale bar, 60 µm; *n* = 6 animals. Arrows, BRG1⁺ cells. **(C)** Diagram showing TAM administration and LPC injection schedule. **(D)** Immunostaining of MBP at lesion sites from control and *Brg1* iKO-*Pdgfra* spinal cords at dpi 14. Scale bar, 50 µm; *n* = 5 animals/genotype. **(E and F)** In situ hybridization for *Mbp* in spinal LPC lesions of control and *Brg1* iKO-*Pdgfra* mice at dpi 14 (E) and dpi 21 (F). Scale bar, 50 µm; *n* = 4 animals/genotype. **(G and H)** In situ hybridization for *Plp1* in spinal LPC lesions of control and *Brg1* iKO-*Pdgfra* mice at dpi 14 (G) and dpi 21 (H). Scale bar, 50 µm; *n* = 4 animals/genotype. **(I)** Quantification of *Plp1*⁺ cells per 0.001 mm^3 in LPC lesion sites. Data are presented as means ± SEM; *n* = 4 animals/genotype. **(J)** Electron microscopy of LPC lesions from control and *Brg1* iKO-*Pdgfra* spinal cords at dpi 14 (left). Quantification of the percentage of remyelinated axons in control and *Brg1* iKO-*Pdgfra* spinal cords at dpi 14 (right). Scale bar, 2 mm; *n* = 4 animals/genotype. **(K)** In situ hybridization for *Pdgfra* in spinal LPC lesions of control and *Brg1* iKO-*Pdgfra* mice at dpi 14 (left). Quantification of *Pdgfra*⁺ cells per 0.001 mm^3 in LPC lesion sites (right). Scale bar, 50 µm; *n* = 4 animals/genotype. Data are presented as mean ± SEM; n.s., not significant; *P < 0.05; **P < 0.01; ***P < 0.001; two-way ANOVA with Sidak's multiple comparisons test (I), two-tailed unpaired Student's *t* test (J and K).

to find that the number of myelinated axons was substantially lower in the lesions of iKO-*Pdgfra* spinal cords at dpi 14 (Fig. 3 J). To rule out the possibility that OPCs were affected in these iKO-*Pdgfra* mice after injury, we performed ISH to label such cells marked by *Pdgrfa* expression and found that the number of *Pdgrfa*⁺ OPCs in the lesion was comparable between iKO-*Pdgfra* and control spinal cords at dpi 14 (Fig. 3 K), suggesting ablation of *Brg1* did not affect OPC recruitment. Taken together, this data demonstrates that BRG1 plays an essential role in OL remyelination after LPC-induced white matter injury.

Brg1 deficiency alters the transcriptional program for OL differentiation

We next sought to define the potential molecular mechanism through which BRG1 drives OPC differentiation into mature OLs. To study this, we isolated OPCs by immunopanning with anti-PDGFRa from P5 control and *Brg1* iKO brain tissues. The isolated OPCs marked by OLIG2 immunostaining were severely impaired in their capacity to differentiate into MBP⁺ mature OLs compared with OPCs from control tissues (Fig. 4 A). When these isolated OPCs were subjected to RNA-sequencing profiling, we

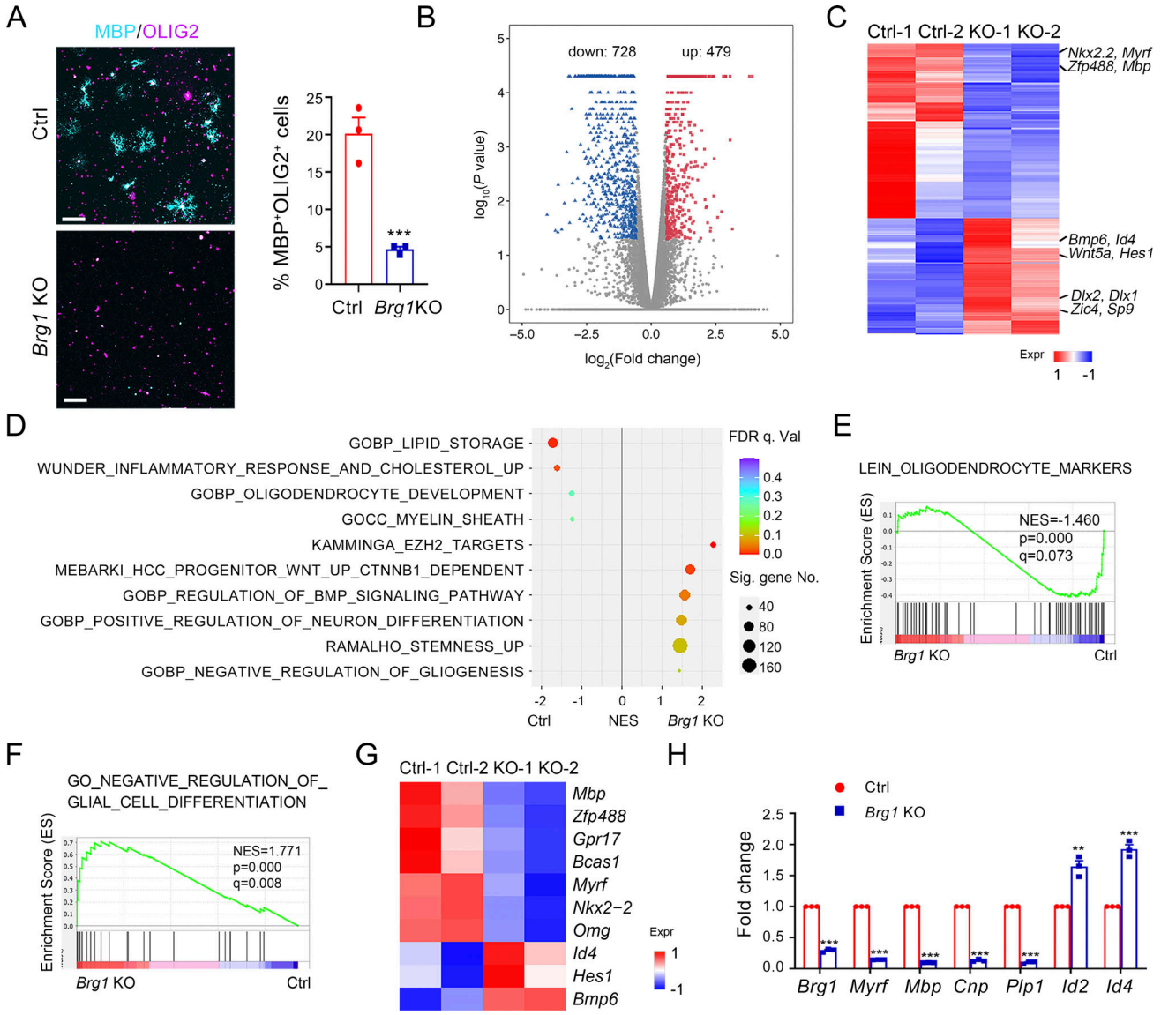

Figure 4. **BRG1 regulates the transcriptional program for OPC differentiation. (A)** Immunostaining (left) and quantification (right) for MBP⁺OLIG2⁺ mature OLs in control and *Brg1* KO OPCs from *Brg1* iKO brains stimulated with T3 for 3 days. Scale bar, 50 µm; *n* = 3 independent experiments. **(B)** Differentially expressed transcripts (highlighted in color; fold change ≥1.5 [$\log_2$(fold change) > 0.585], false discovery rate <0.05) between OPCs isolated from control and *Brg1* iKO mouse brains at P7. *n* = 2 independent experiments. **(C)** Heatmap shows differentially expressed genes in *Brg1* KO OPCs compared with control OPCs. *n* = 2 independent experiments. **(D)** GSEA of genes enriched in control or *Brg1* KO OPCs; NES, net enrichment score. **(E and F)** GSEA plots of *Brg1* KO OPCs show downregulation of oligodendrocyte markers signature and upregulation of negative regulation of glial cell differentiation signature. **(G)** The heatmap shows the indicated differentially expressed oligodendrocyte genes in *Brg1* KO OPCs compared with control OPCs. *n* = 2 independent experiments. **(H)** qPCR analysis of OPC differentiation-associated genes in control and *Brg1* KO OPCs. *n* = 3 independent experiments. Data are presented as mean ± SEM; ***P < 0.001; two-tailed unpaired Student's *t* test (A and H).

found that *Brg1* deficiency in OPCs led to a set of significantly upregulated and downregulated genes with changes in expression levels of 1.5-fold or greater (P < 0.05) (Fig. 4, B and C; and Table S1). Gene Set Enrichment Analysis (GSEA) revealed that the genes downregulated in *Brg1* knockout OPCs were enriched in those associated with the regulation of glial cell differentiation including OL differentiation genes (Fig. 4, D–F), consistent with the dysmyelination phenotype in *Brg1* iKO-*Pdgfra* mice. Further, expression levels for mature OL markers such as *Zfp488*, *Myrf*, *Nkx2-2*, and *Mbp* were reduced in *Brg1* knockout OPCs compared with control, whereas OPC differentiation inhibitory genes such as *Hes1*, *Id4*, and *Bmp6* were upregulated (Fig. 4 G). Quantitative real-time PCR analysis further confirmed the reductions in expression levels for OL differentiation-associated genes *Cnp*, *Myrf*, *Mbp*, *Plp1*, as well as corresponding increased expression levels for differentiation inhibitory genes *Id2* and *Id4* in *Brg1*-deficient OPCs (Fig. 4 H). Overall, these data demonstrate that loss of Brg1 impedes expression of OL differentiation-promoting regulators while increasing the genes that suppress differentiation.

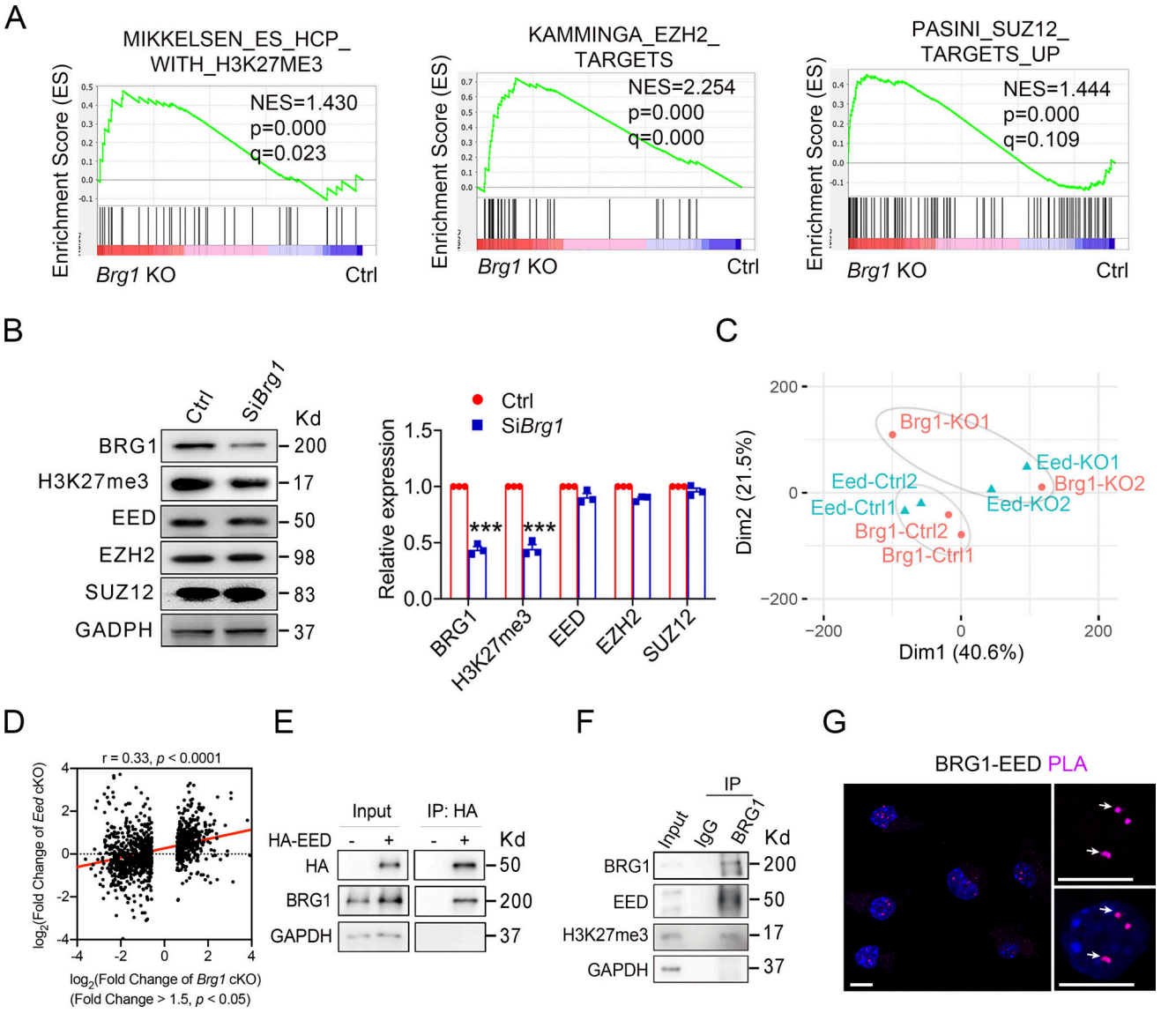

Figure 5. **BRG1 binds with and promotes PRC2 activity in OPCs. (A)** GSEA plots of H3K27me3, EZH2 targets, and SUZ12 targets enriched in *Brg1* KO OPCs. **(B)** Western blot (left) and quantification (right) of BRG1, EED, EZH2, SUZ12, H3K27me3, and GAPDH from lysates of control and Si*Brg1* treated Oli-neu cells. *n* = 3 independent experiments. **(C)** PCA plot of expression profiles of *Brg1* KO OPCs (red) and *Eed* KO OPCs (blue). **(D)** Correlation of significantly changed gene expression in *Eed* KO OPCs and gene expression changes in *Brg1* KO OPCs. Correlation and P values were obtained from Pearson's product-moment correlation. **(E)** Coimmunoprecipitation assay for BRG1 and HA antibodies in Oli-neu cells transfected with plasmids expressing HA-tagged EED. *n* = 3 independent experiments. **(F)** Co-immunoprecipitation assay for BRG1, EED, and H3K27me3 antibodies in primary mouse OPCs. *n* = 3 independent experiments. **(G)** Representative images showed the proximity ligation assay of the BRG1-EED interaction (arrow) in primary mouse OPCs. *n* = 3 independent experiments. Scale bars, 10 µm. Data are presented as mean ± SEM; ***P < 0.001; two-tailed unpaired Student's *t* test (B). Source data are available for this figure: SourceData F5.

BRG1 interacts with PRC2 to reprogram H3K27me3 in OPCs

Polycomb repressive complex 2 (PRC2) is a sole chromatin modifier that catalyzes the repressive histone mark H3K27me3 (Yu et al., 2019). Intriguingly, GSEA revealed that the gene signatures of chromatin remodeling, H3K27me3 and the targets of EZH2 or SUZ12, the core subunits of PRC2 (Yu et al., 2019), were enriched in *Brg1*-knockout OPCs (Fig. 4 D and Fig. 5 A). This suggested that the genes suppressed by H3K27me3 and PRC2 were upregulated in *Brg1*-deficient OPCs. Although the protein levels of EED, EZH2, and SUZ12 were comparable in si*Brg1*-treated and control siRNA-treated OPCs, the expression level for H3K27me3 was substantially reduced in si*Brg1*-treated OPCs (Fig. 5 B), suggesting that *Brg1* knockdown interfered with PRC2 activity without significantly altering PRC2 steady-state levels in OPCs. Principal component analysis of transcriptional control networks indicated that the gene profiles of the transcriptome of *Brg1*-knockout OPCs were more closely related to those of *Eed*-knockout OPCs than of control OPCs (EED^{wt} or $BRG1^{wt}$) (Fig. 5 C), suggesting that BRG1 and EED/PRC2 complexes modulate common downstream pathways. Furthermore, gene expression changes in *Brg1*-deficient OPCs were positively correlated to those in *Eed*-deficient OPCs (Fig. 5 D).

BRG1 has previously been shown to promote PRC2-mediated repression during stem cell lineage commitment (Alexander

et al., 2015; Ho et al., 2011; Menon et al., 2019). To determine if BRG1 regulates PRC2 functions through protein–protein interaction, we performed co-immunoprecipitation by expressing HA-tagged EED in a mouse OL cell line Oli-neu under differentiating conditions (Söhl et al., 2013). As shown in Fig. 5 E, we found that EED was coimmunoprecipitated with endogenous BRG1, suggesting that BRG1 is present and able to form protein complexes with EED/PRC2 in the mouse OL cell line. Additionally, we demonstrated that endogenous BRG1 also co-immunoprecipitated with EED and H3K27me3 in primary mouse OPCs (Fig. 5 F), confirming the interaction between BRG1 and EED/PRC2 in OPCs. This is in keeping with the observations of cooperativity between BRG1 and PRC2 for gene repression in other cell types (Alexander et al., 2015; Li et al., 2017). Furthermore, we performed a proximity ligation assay (in situ PLA) to determine if BRG1 and EED physically interact. BRG1 and EED were detected in the same foci in the nuclei of primary OPCs (Fig. 5 G). Taken together, these data indicate that BRG1 can directly interact with EED and may cooperate with the EED/PRC2 complex to regulate transcriptional programs for OPC differentiation.

Brg1 loss derepresses H3K27me3 occupied genes associated with the inhibition of OPC differentiation

Recent studies indicate that the BRG1-BAF complex is required for Polycomb/PRC2-mediated gene repression during lineage differentiation from stem/progenitor cells (Alexander et al., 2015; Ho et al., 2011; Weber et al., 2021), in addition to its role antagonizing PRC2 functions in other contexts. We found that the expression levels for genes with high SUZ12 and H3K27me3 occupancy were increased in *Brg1*-deleted OPCs (as assessed by normalized peak counts), suggesting that such genes were derepressed following *Brg1*-deletion in OPCs (Fig. 6 A). PRC2-targeted genes elevated in *Brg1*-depleted OPCs included WNT and bone morphogenetic protein (BMP) signaling pathway regulators, *Lef1* and *Bmp6* (Fig. 6, B and C). Consistently, GSEA showed that the genes upregulated in *Brg1*-deficient OPCs were enriched in WNT and BMP signaling pathways (Fig. 6 D), which are the negative regulators of OL differentiation (Azim and Butt, 2011; Samanta and Kessler, 2004). qPCR analysis confirmed the upregulation of the WNT (e.g., *Lef1*, *Tcf3*) and BMP signaling pathway regulators (e.g., *Id2*, *Id4*) in *Brg1*-deficient OPCs (Fig. 6 E and Fig. 4 H). To determine the H3K27me3 occupancy on the promoter region of WNT and BMP signaling regulators, *Lef1* and *Bmp6*, we performed ChIP-qPCR analysis and found that H3K27me3 recruitment to the promoter region of *Lef1* and *Bmp6* was substantially reduced upon *Brg1* knockdown (Fig. 6 F). Together, these data indicate that *Brg1* deficiency results in disinhibition of H3K27me3/PRC2 occupied genes associated with WNT and BMP signaling pathways, suggesting that the BRG1/BAF complex is required for PRC2-mediated repression of the genes that inhibit OPC differentiation.

Neuronal differentiation genes upregulated in *Brg1*-deficient OPCs inhibit myelination programs

BRG1 has been shown to be critical for sustaining gliogenesis from neural progenitor cells, and the loss of *Brg1* in NSCs results in precocious neuronal differentiation (Matsumoto et al., 2006). Intriguingly, we found that the genes upregulated in *Brg1*-deleted OPCs were enriched in gene signatures associated with neuronal differentiation and neurogenesis (Fig. 7 A). Consistently, transcriptomic analyses and qPCR experiments demonstrated that the expression levels for neuronal differentiation genes (*Dlx2*, *Pou3f3*, and *Gsx2*) were elevated in *Brg1*-deficient OPCs (Fig. 7 B), while the expression of astrocyte gene *Gfap* was not altered (Fig. 7 C). Notably, the expression levels for neuronal specification genes such as *Sp9* and *Zic4* were upregulated in *Brg1*-deficient OPCs (Fig. 6 A and Fig. 7 C). SP9 and ZIC4 have been shown to promote neuronal cell fate specification and differentiation (Elsen et al., 2008; Li et al., 2018). The promoter elements *Sp9* and *Zic4* exhibited intense occupancy by SUZ12 and H3K27me3 in OPCs (Fig. 7 D). We further performed ChIP-qPCR and found that H3K27me3 occupancy on such promoter regions was reduced in *Brg1*-knockdown OPCs (Fig. 7 E). This suggests that the loss of *Brg1* in OPCs leads to derepression of H3K27me3-occupied *Sp9* and *Zic4*. Moreover, we found that *Sp9* overexpression led to decreased promoter activity of *Mbp*, while *Zic4* overexpression resulted in attenuated promoter activity of *Olig2* in luciferase reporter assays (Fig. 7 F), suggesting that the upregulated expression of neuronal genes *Sp9* and *Zic4* could inhibit expression of the myelination program in *Brg1*-deficient OPCs. Thus, our data suggest that BRG1 is required for maintaining H3K27me3/PRC2-mediated repression of neuronal lineage differentiation genes to inhibit alternative fates of OPCs (Fig. 7 G).

Discussion

Critical role of BRG1 in OPC differentiation in the postnatal developing brain

BRG1 is highly expressed in OPCs during development and is downregulated in mature OLs. Our previous study showed that deletion of *Brg1* using OL lineage–expressing Olig1-Cre, starting at the pri-OPC stage prior to the committed OPCs, led to a marked impairment in OL differentiation in the CNS, resulting in severe hypomyelination (Yu et al., 2013). However, the role of BRG1 in the differentiation from committed OPCs in the postnatal developing brain has not been fully defined previously. Our present study using a developmentally regulated *PDGFRa-CreERT* driver for *Brg1* ablation specifically in OPCs reveals a pivotal function of BRG1 for OPC differentiation during postnatal brain development. This is in contrast to the nuanced yet significant impact of Brg1 ablation using NG2-Cre or CNP-Cre drivers in the developing spinal cord (Bischof et al., 2015). Our findings suggest an essential role of BRG1 in OPC differentiation and subsequent myelination during brain development, demonstrating a region-specific impact of BRG1 on OL lineage progression between the developing brain and spinal cord.

Stage- and region-specific impact of BRG1 loss on OPC differentiation

In the developing brain, *Brg1* deletion in OPCs, directed by a *Pdgfra-CreERT* line, results in severe defects in OL differentiation and subsequent myelination, similar to the phenotype with

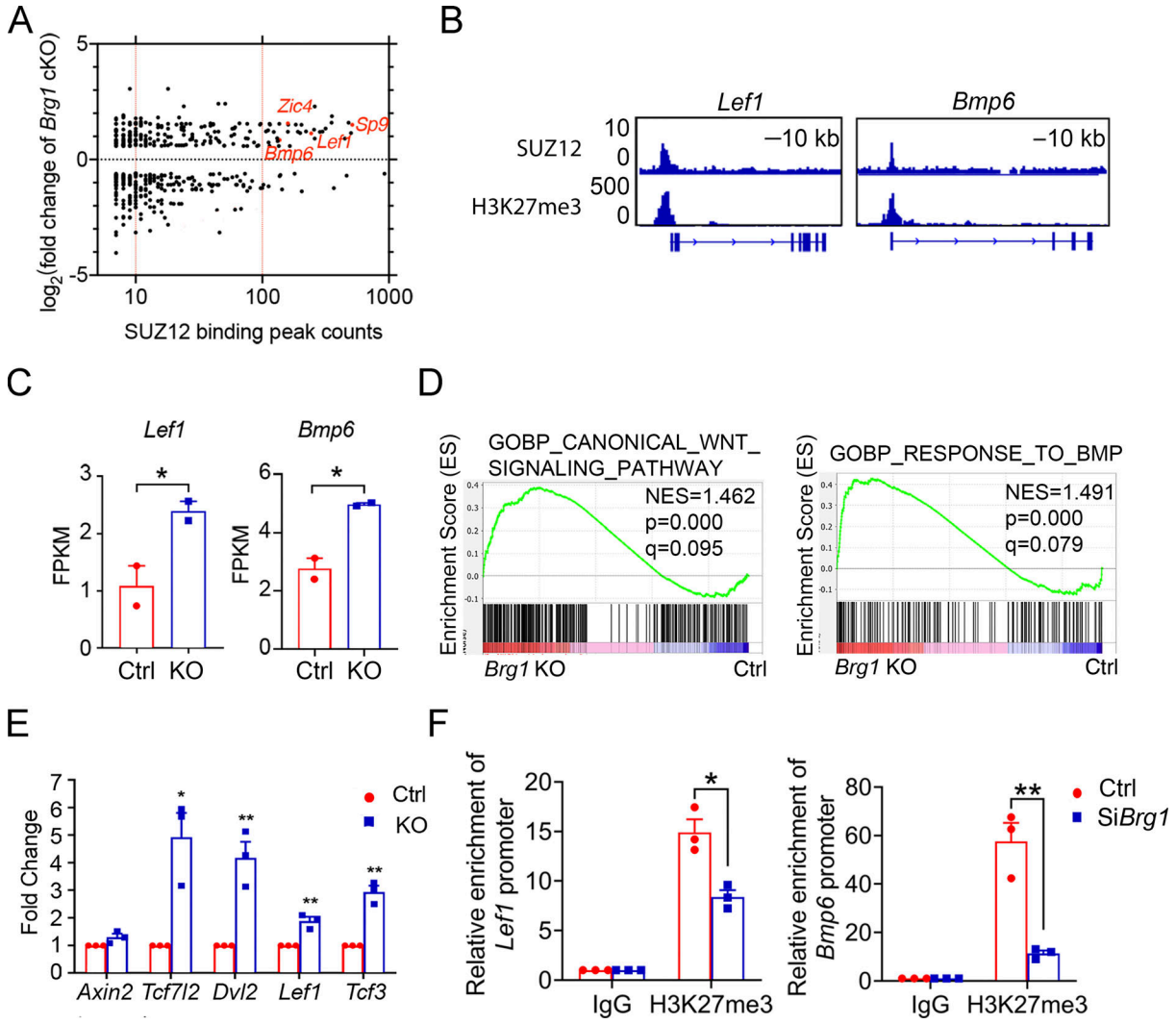

Figure 6. **BRG1 interacts with PRC2 to suppress negative regulators of OPC differentiation. (A)** Bland–Altman plot showing genome-wide changes to SUZ12 ChIP-seq peaks in OPCs with significant gene expression change in *Brg1* KO OPCs isolated from *Brg1* iKO mice. **(B)** Representative SUZ12 and H3K27me3 ChIP-seq peak tracks of high-binding genes like *Lef1* and *Bmp6* in OPCs, visualized by the Integrative Genome Viewer (IGV) software. **(C)** Fold change of *Lef1* and *Bmp6* genes in RNA-seq of control and *Brg1* KO OPCs. **(D)** GSEA plots of gene signatures with WNT signaling pathway and BMP response enriched in *Brg1* KO OPCs. **(E)** qPCR analysis of WNT signaling pathway genes in control and *Brg1* KO OPCs. *n* = 3 independent experiments. **(F)** ChIP-qPCR analysis of H3K27me3 enrichment at the promoter region of the *Lef1* (left) and *Bmp6* (right) genes in control and Si*Brg1*-treated Oli-neu cells. *n* = 3 independent experiments; IgG, immunoglobulin G. Data are presented as mean ± SEM; *P < 0.05; **P < 0.01; two-tailed unpaired Student's *t* test (C, E, and F).

Brg1 deletion by *Olig1-Cre* (Yu et al., 2013). However, these defects were less severe in the developing spinal cord compared with the brain. This finding aligns with the observation that *Brg1* deletion by a *Ng2-Cre* line results in a moderate reduction of differentiated OLs in the spinal cord (Bischof et al., 2015). The mechanisms underlying the CNS region-specific effects of BRG1 loss on OPC differentiation between the brain and spinal cord remain to be determined. Given that OLs in the brain develop later and exhibit distinct characteristics compared with those in the spinal cord (Bergles and Richardson, 2015; Floriddia et al., 2020; Khandker et al., 2022), the developmental timing and the heterogeneity of OL lineage cells in the spinal cord and brain may account for the difference in severity of the Brg1 mutant phenotypes. Thus, this discrepancy could arise from the spatiotemporal-specific impact of BRG1 on OPC differentiation within the CNS, differentiating between the brain and spinal cord.

In the developing spinal cord, *Brg1* ablation with OL lineage-expressing *Olig1-Cre* starting at the pri-OPC stage leads to severe OL deficits and dysmyelination (Yu et al., 2013). On the other hand, deletion of *Brg1* directed by *NG2-Cre* or *Cnp-Cre*, which induces gene loss in immature OLs, results in a nuanced yet significant decrease in the number of mature OLs at the postnatal stage (Bischof et al., 2015). Furthermore, we find that *Brg1* deletion in *Cnp+* immature OLs at the embryonic stage causes an OL differentiation defect in the developing spinal cord. This indicates that BRG1 has a stage-specific role in OL lineage differentiation within the developing spinal cord. Notably, we observed more pronounced defects in OPC differentiation in the spinal cord following ablation of *Brg1* in *Pdgfra-CreERT* mice

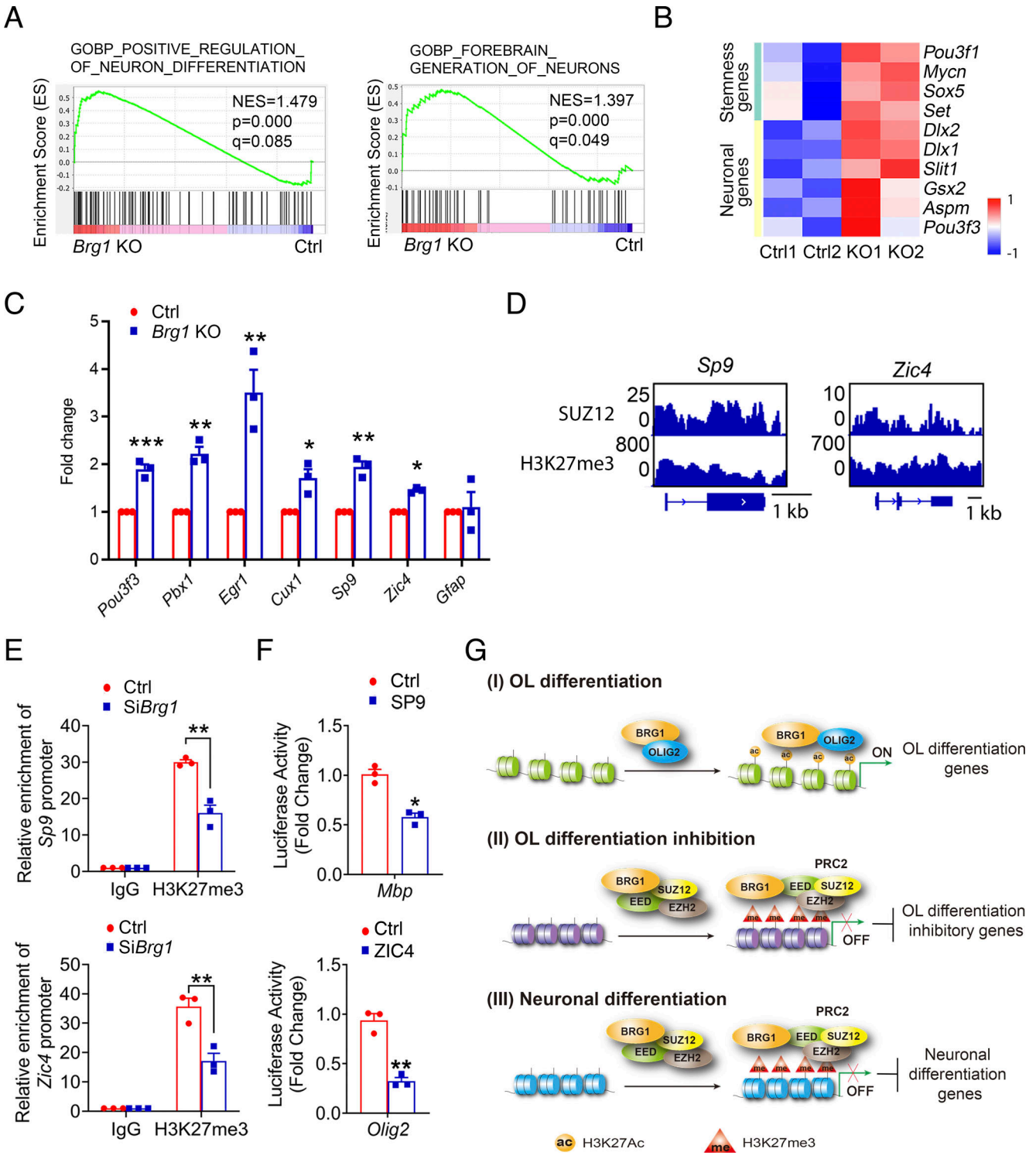

Figure 7. **BRG1 cooperates with PRC2 to suppress neuronal gene expression within OPCs. (A)** GSEA plots of neuron differentiation-related gene signatures enriched in *Brg1* KO OPCs. **(B)** Heatmaps of Stemness genes and neuronal genes in control and *Brg1* KO OPCs. **(C)** qPCR analysis of neuronal genes and astrocyte genes in control and *Brg1* KO OPCs. *n* = 3 independent experiments. **(D)** Representative SUZ12 and H3K27me3 ChIP-seq peak tracks of neuronal genes like *Sp9* and *Zic4* in OPCs, visualized by the IGV software. **(E)** ChIP-qPCR analysis of H3K27me3 enrichment at the promoter region of the *Sp9* and *Zic4* genes in control and Si*Brg1*-treated Oli-neu cells. *n* = 3 independent experiments; IgG, immunoglobulin G. **(F)** Luciferase analysis of the promoter region of *Mbp* or *Olig2* in control, *Sp9* and *Zic4* overexpressed Oli-neu cells. *n* = 3 experiments. **(G)** A schematic diagram of BRG1 function during OL differentiation. **(I)** BRG1 is recruited by the transcription factor OLIG2 to activate the expression of OL differentiation genes. **(II)** BRG1 interacts and promotes PRC2-mediated repression at OL differentiation inhibitory genes. **(III)** BRG1 interacts and promotes PRC2-mediated repression at non-OL neuronal genes. Data are presented as mean ± SEM; *P < 0.05; **P < 0.01; ***P < 0.001; two-tailed unpaired Student's *t* test (C, E, and F).

compared with those in *NG2*-Cre mice. The precise mechanism underlying this discrepancy remains to be defined. The difference in the Cre recombination efficiency between these deleter lines might contribute to phenotypic variations in severity, given that *Ng2-Cre* exhibits a low Cre recombination efficiency and only recombines floxed alleles in a small fraction of OPCs (<4%, 27%, and 50 % at 14.5, 16.5 day post-coitum, and P14, respectively) (Bischof et al., 2015), while *Pdgfra-CreERT* can achieve nearly 90% recombination efficiency (O'Rourke et al., 2016). Thus, in the case of *Ng2-Cre*-mediated *Brg1* depletion, the low efficiency in *Brg1* deletion may lead to a compensatory expansion of OPCs that escaped from *Brg1* loss. Nonetheless, our analysis with the reporter of Cre recombination demonstrates that deletion of *Brg1* in PDGFRα⁺ OPCs in vivo impedes their differentiation and subsequent myelination, highlighting a requirement of BRG1 for proper OPC differentiation in both the brain and spinal cord.

Consistent with the stage-specific role of BRG1, in the early embryonic spinal cord, we showed that *Brg1* deletion in *Cnp*⁺ immature differentiating OLs led to a differentiation defect, but this defect was less severe at the postnatal stages. The phenotypic differences following *Brg1* ablation suggest a temporally specific function of BRG1 in OL lineage progression in the developing spinal cord. The differential severity of dysmyelination observed with *Brg1* ablation at different lineage stages may be reflective of the differences in the functions for BRG1 in *PDGFRα*⁺ OPCs compared with *Cnp*⁺ differentiating OLs. This suggests that once differentiating OLs acquire characteristics of open chromatin, such as transcription factor binding and H3K27ac enhancer establishment, they might be less dependent on BRG1 in maintaining these characteristics for subsequent myelination. Together, these observations suggest a region- and stage-dependent BRG1 function for OL lineage differentiation.

BRG1 differentially modulates OL and neuronal differentiation programs to ensure OL lineage progression

The interaction between chromatin remodeling complexes, such as the BRG1 SWI/SNF complex, and histone modifications is key for OL lineage progression (Berry et al., 2020; Emery and Lu, 2015). The BRG1-SWI/SNF complex, a Trithorax-group homolog, is involved in the de novo activation of transcription to regulate the neural developmental process (Fletcher et al., 2017; Sokpor et al., 2017). Our previous study indicates that BRG1 can target the activating H3K27ac-marked enhancers of OL regulatory genes at the onset of OPC differentiation (Yu et al., 2013). Moreover, BRG1 can be transcriptionally recruited by the pioneer transcription factor OLIG2 in the OL lineage to achieve target binding specificity, and to activate expression of OL-differentiation-associated programs (Yu et al., 2013). However, BRG1 is also required for the repression of a diverse group of developmental regulators in a cell-context-dependent manner (Seeker et al., 2023; Weber et al., 2021). BRG1-containing SWI/SNF complex can function as both an activator or a repressor of target genes by reshaping the nucleosome landscape (Ho and Crabtree, 2010; Liu et al., 2011). In the present study, we demonstrated that BRG1 regulates OPC differentiation by activating the expression of OPC differentiation genes while repressing the expression of inhibitors of OL differentiation, as well as genes associated with neuronal differentiation. These observations suggest that BRG1 plays a dual function in OPC differentiation. It can enhance OPC differentiation by activating OL lineage regulatory genes through interactions with their enhancers while repressing inhibitors of OL differentiation as well as neuronal differentiation genes to ensure proper lineage commitment.

BRG1 interacts with EED/PRC2 repressive complexes to safeguard OL lineage progression

Strikingly, we found that BRG1 is essential for PRC2-mediated repression of genes inhibiting OPC differentiation. Our transcriptome profiling analysis reveals that *Brg1* deficiency disrupts the repression of PRC2/H3K27me3 occupied genes associated with the inhibition of OPC differentiation, suggesting that BRG1 is required for PRC2-mediated repression of inhibitory programs that hinder OPC differentiation. Further, we show that BRG1 can interact directly and cooperate with PRC2 to deposit the repressive mark H3K27me3 on the promoters of OL differentiation inhibitory genes as well as neuron differentiation genes, thereby facilitating OPC differentiation and suppressing alternative neuronal pathways. This is in keeping with studies in other cellular contexts showing that BRG1 can cooperate with PRC2 to enhance gene repression (Alexander et al., 2015; Li et al., 2017). As such, cooperativity between BRG1/BAF (BRG1/BRM-associated factor) and PRC2 complexes may selectively regulate the activity of BAF complexes, guiding the differentiation of multiple distinct cell lineages. Our studies indicate that BRG1-dependent chromatin remodeler has a dual role in OL lineage progression by cooperating with OL lineage specification factors such as Olig2 to promote OL differentiation while enhancing PRC2-mediated repression on expression of differentiation inhibitors and neuronal programs (Fig. 7 G). Congruently, in the developing embryonic cortex, BRG1 is required for neuroepithelial-to-radial glial cell transition and OPC specification. It can also inhibit the expression of Olig2 in a population of cortical neural progenitors while promoting the expression of neurogenic factors, such as Pax6, for neuronal differentiation (Matsumoto et al., 2016). These observations highlight dynamic, lineage-specific mechanisms of BRG1-BAF for controlling OL and neuronal lineage development. Our findings reveal that the dynamic epigenetic interplay between chromatin remodeling complexes and histone modifications is crucial for maintaining faithful and robust gene expression programs that drive OL lineage commitment and differentiation.

A critical role of BRG1 in myelin regeneration and diseases

In addition to the critical role that BRG1 plays in regulating OPC differentiation in both the brain and spinal cord, albeit to varying degrees, during normal myelination, we demonstrated that BRG1 is required for PDGFRα⁺ OPC remyelination in the spinal cord following demyelinating injury. However, its role in OL remyelination after brain injury remains to be defined. Given the importance of BRG1 in tissue regeneration (Li et al., 2019; Xiao et al., 2016; Xiong et al., 2013), our findings underscore the potential significance of BRG1 in CNS repair following injury. This insight opens avenues for developing future therapies

aimed at treating demyelinating diseases. Additionally, *BRG1* mutations have been linked to Coffin-Siris syndrome (CSS) (Li et al., 2020; Tsurusaki et al., 2012), a rare congenital abnormality with clinical characteristics such as intellectual disability, progressive coarsening of the face, hypertrichosis, and frequent infections. Notably, CSS patients with *BRG1* mutations frequently exhibit white matter defects and partial agenesis of the corpus callosum (Vasko et al., 2021), suggesting a critical role of BRG1 for white matter development in the CNS. Given the established critical role of BRG1 in OPC differentiation in the developing brain, mutations in BRG1/SMARCA4 could directly impact the myelination process, leading to white matter anomalies in CSS patients. Collectively, our findings suggest that BRG1 may have an important role in myelin regeneration, which could be pivotal in addressing demyelinating and other neurodegenerative diseases.

Materials and methods

Mouse line and genotyping

The *Brg1* loxp-flanked mice were crossed with *Pdgfra-CreERT* and tdTomato reporter mice to generate OPC-specific *Brg1* iKO-*Pdgfra* (*Pdgfra-CreERT*; *Brg1*$^{flox/flox}$; tdTomato) and heterozygous control (*Pdgfra-CreERT*; *Brg1*$^{flox/+}$; tdTomato) mice. *Cnp-Cre* mice were crossed with *Brg1*$^{flox/flox}$mice to generate *Brg1* cKO-*Cnp* mice (*Cnp-Cre*$^{+/-}$; *Brg1*$^{flox/flox}$). Both male and female mice used in the experiments were maintained on a mixed C57/BL6; 129Sv background. All animal experiments were approved by the Institutional Animal Care and Use Committee (IACUC) of Cincinnati Children's Hospital Medical Center.

Brg1$^{flox/flox}$ line was genotyped using primers 5′-TCTCATG CACAGAGGTCCTG-3′ and 5′-TAGCCCCTTGAAAGTGATCC-3′. Mice positive for the *Pdgfra-CreERT* transgene were identified with the primers 5′-ATCCTGATGATTGGTCTCGTCT-3′ and 5′-TGTTACTCATGTGCCTGATGTG-3′. The tdTomato reporter line was genotyped using primers 5′-AAGGGAGCTGCAGTGGAGTA-3′, 5′-CCGAAAATCTGTGGGAAGTC-3′, 5′-CTGTTCCTGTACGGC ATGG-3′, and 5′-GGCATTAAAGCAGCGTATCC-3′. The *Cnp-Cre* line was identified with the primers 5′-GGACATGTTCAGGGATCG CCAGGCG-3′ and 5′-GCATAACCAGTGAAACAGCATTGCTG-3′.

Tamoxifen-induced ablation of *Brg1* in postnatal OPCs and adult OPCs

Tamoxifen (T5648; Sigma-Aldrich) was dissolved in 90% sunflower oil and 10% ethanol to 5 mg/ml and 10 mg/ml. Newborn pups were given a daily intraperitoneal injection of 0.1 mg tamoxifen for three consecutive days. Adult mice were treated with tamoxifen (100 mg/kg) daily for five consecutive days.

Tissue processing, immunostaining, and microscopy

Mice at different developmental stages were anesthetized with ketamine and xylazine and perfused with PBS followed by 4% paraformaldehyde (PFA). Brains and spinal cords were removed, postfixed in 4% PFA for 1 h, sunk in 25% sucrose overnight at 4°C, and embedded in OCT and cryosectioned at 16 µm.

Sections were permeabilized and blocked in 5% normal donkey serum with 0.2% Triton X-100 for 1 h at room temperature and stained overnight at 4°C with primary antibodies as follows: rabbit anti-OLIG2 (AB9610; Millipore, RRID: AB_570666), rat anti-PDGFRα (558774; BD Bioscience, RRID: AB_397117), mouse anti-APC (CC1, OP80; Millipore, RRID: AB_2057371), goat anti-MBP (sc-13914; Santa Cruz Biotechnology, RRID: AB_648798), rabbit anti-BRG1 (sc-10768; Santa Cruz Biotechnology, RRID: AB_2255022), mouse anti-GFAP (G3893; Sigma-Aldrich, RRID: AB_477010), rabbit anti-Ki67 (RM-9106; Thermo Fisher Technology, RRID: AB_2335745), rabbit anti-cleaved caspase 3 (#9661; Cell Signaling Technology, RRID: AB_2341188), and rabbit anti-Iba1 (019-19741; Wako Pure, RRID: AB_839504). Sections were then incubated with the appropriate fluorescent conjugated antibodies (Jackson ImmunoResearch Laboratories) for 1.5 h at room temperature, stained in DAPI for 5 min, washed in PBS, and mounted with Fluoromount-G (0100-01; SouthemBiotech).

Images were captured using Nikon C2+ confocal microscopy system at room temperature and analyzed using NIS-elements and ImageJ software (National Institutes of Health).

In situ mRNA hybridization

In situ hybridization was performed as described previously (Wang et al., 2020). Cryostat sections (16 µm) were thaw-mounted onto Superfrost slides (12-550-15; Fisherbrand), allowed to dry at room temperature (RT), and then stored at −20°C. To prepare for processing, the slides were warmed to RT and subsequently dried at 50°C for 15 min. They were then fixed in 4% paraformaldehyde in DEPC-treated PBS (DepC-PBS) at RT for 20 min, followed by two washes in DepC-PBS at RT for 5 min each. The sections were treated with 10 µg/ml proteinase K for 12 min, then washed once in DepC-PBS at RT for 5 min, and fixed again in 4% paraformaldehyde in DepC-PBS for 15 min. After rinsing twice in DepC-Water, slides were placed in an RNAse-free glass trough with a stir bar and 200 ml 0.1 M RNAse-free triethanolamine-HCl pH 8.0. 0.5 ml acetic anhydride was added into a glass trough with constant stirring for a further 10 min. The slides were washed in DepC-PBS at RT for 5 min before prehybridization, which occurred for 1–4 h at 65°C in hybridization buffer (50% formamide, 5X SSC, 0.3 mg/ml yeast tRNA, 100 µg/ml heparin, 1X Denhardt's, 0.1% Tween, 0.1% CHAPS, and 5 mM EDTA). This was replaced with 1–2 µg/ml of the probe in hybridization buffer, continuing the incubation for 12–16 h. Slides were then transferred to a glass trough and washed once in 250 ml of 2X SSC for 15 min in a 65°C oven with stirring. This was followed by the addition of 0.2 µg/ml RNase A to 2X SSC, incubating at 37°C for 30 min, and then rinsing twice with 1X SSC at RT and washed with 0.2X SSC at 65°C for 15 min, and then two subsequent washes for 30 min each in an oven with a stir bar. For blocking, slides were treated with PBT+10% heat-inactivated sheep serum for 30 min to an hour at RT and then placed flat in a humidified chamber. Each slide received 400 µl of embryo-powder preabsorbed anti-digoxigenin antibody (diluted 1:2,000 in PBT+1% sheep serum) and was incubated for 30 min to 2 h at RT or overnight at 4°C. This was followed by three washes in PBT for 30 min each at RT, and two washes in alkaline-phosphatase buffer for 5 min each at RT. To each ml of alkaline-phosphatase buffer, 1 µl of NBT (nitro blue tetrazolium; 11383213001; Sigma-Roche) and 3.5 µl of BCIP (5-bromo-4-

chloro-3-indolyl phosphate; 10760978103; Sigma-Roche) were added, and development occurred in the dark for 2–20 h, depending on RNA abundance. After three washes in PBS to remove substrates, the sections were fixed in 4% paraformaldehyde for more than 15 min, embedded in 100% glycerol with a coverslip, and sealed with nail polish. Digoxigenin (DIG)-labeled antisense riboprobes against *Mbp*, *Plp1*, and *Pdgfra* were synthesized with T3 or T7 RNA polymerase (P207B and P2083; Promega) and labeled with DIG RNA Labeling Mix (Cat#11 277 073 910; Roche).

In situ proximity ligation assays (PLA)

Primary OPCs were fixed and permeabilized in preparation for PLA (Duolink In Situ Detection Reagents Red—DUO92008; Sigma-Aldrich) according to the manufacturer's instructions. Cells were incubated with primary antibodies for mouse anti-BRG1 (sc-17796; Santa Cruz Biotechnology, RRID: AB_626762) and rabbit anti-EED (85322; Cell Signaling Technology, RRID: AB_2923355). The cells were washed and then treated with the PLA probe and secondary antibodies directly conjugated with oligonucleotides (PLA probe MINUS and PLA probe PLUS), followed by adding a ligation solution, consisting of two oligonucleotides and ligase. The oligonucleotides will hybridize with the PLA probe and join to form a circle if in close proximity. An amplification solution is then added containing fluorescently labeled oligonucleotides and a polymerase. The oligonucleotide arm of one of the PLA probes acts as a primer for "rolling-circle amplification" (RCA) using the ligated circle as a template, and this generates a repeated concatemeric product. The fluorescently labeled oligonucleotides then hybridized to the RCA product which was analyzed by confocal microscopy. Nuclei were counterstained with DAPI.

Transmission electron microscopy

Tissue processing was performed as described previously (Wang et al., 2020). Briefly, mice were deeply anesthetized with ketamine and xylazine and transcardially perfused with 0.1 M cacodylate, followed by 4% PFA/2.5% glutaraldehyde in 0.1 M cacodylate (pH 7.4). Brain and spinal cord were dissected and postfixed for 48 h in this fixative buffer before being processed for embedding. Semithin sections were cut and stained with toluidine blue to evaluate the quality and orientation of the tissue. Ultrathin sections were cut on chosen samples for electron microscopy imaging.

Lysolecithin-induced demyelinating injury

Lysolecithin-induced demyelination was carried out in the ventrolateral white matter of the spinal cord as previously described (Wang et al., 2020). In brief, 8–10 wk-old control and *Brg1* iKO-*Pdgfra* mice were anesthetized and maintained by 2% isoflurane. After exposing the spinal vertebrae at the level of T3-T4, meningeal tissue in the intervertebral space was cleared, and the dura was pierced with a dental needle. 0.5 µl of 1% lysolecithin was injected into the ventrolateral white matter using a stereotactic manipulator. Injuries were conducted in a genotype-blinded manner. Tissues carrying injured lesions were harvested at different time points.

Primary mouse OPC culture

Mouse OPCs were isolated from P5-P6 cortices of mice by immunopanning with antibodies against RAN-2, GalC, and O_4 sequentially as described previously (Emery and Dugas, 2013). Mouse cortices were dissected in D-PBS without Ca^{2+}/Mg^{2+} in the dish and the tissue was diced into 1 mm^3 chunks. The tissue was then digested and triturated in a papain solution in a sterile 50-ml conical tube. Upon completion of the digestion, papain solution was removed and 2 ml of low-ovo solution with DNase I was added to the tissue. Subsequently, the low-ovo solution was removed and discarded. Next, another 2 ml of low-ovo solution with DNase I was added and the tissue was dissociated twice. The cells were pelleted at 300 × *g* for 15 min and the supernatant was aspirated. The cell pellet was resuspended in 6 ml of high-ovo solution and immediately pelleted again. After aspirating the supernatant, the cell pellet was resuspended in 5 ml of panning buffer and the cells were filtered into a new tube. Lastly, the cells were pelleted and resuspended and OPCs were obtained by immunopanning with antibodies against NG2, GalC, and O4, sequentially. The isolated mouse OPCs were cultured in a Sato growth medium supplemented with B27, NT3, Forskolin, and PDGFAA at 37°C and 10% CO_2. 50% of the medium was replaced with fresh medium every 2 days.

RNA isolation and quantitative real time-PCR

RNA from purified mouse OPCs from control or *Brg1* iKO-*Pdgfra* mice brains was extracted using TRIZOL (Life Technologies). First-strand cDNA synthesis was performed using iScript Reverse Transcription Supermix (BioRad) and was amplified using quantitative SYBR green PCR mix (BioRad) according to the manufacturer's instructions. qRT-PCR was performed using the StepOnePlus Real-Time PCR System (Applied Biosystems). PCR primers were designed using IDT. Expression values for each gene were normalized against *gapdh* using the delta-delta CT method. PCR primer sequences are listed in Table S2.

RNA-seq and data analysis

RNA was extracted from control and *Brg1* KO OPCs using the QIAGEN RNeasy Micro Kit. RNA-seq libraries were prepared using SMART-Seq v4 Ultra Low Input RNA Kit. Massively parallel 101 bp PE sequencing was completed on an Illumina HiSeq2500 to acquire ~25 M fragments per sample.

The RNA sequencing files were cleaned to keep high quality reads using both FastQC (https://www.bioinformatics.babraham.ac.uk/projects/fastqc/) and CutAdapt 1.3 (https://pypi.python.org/pypi/cutadapt) software. The sequences of the reads containing unknown base N and reads with more than 10% Q < 20 bases were eliminated. RNA sequencing files were mapped to the genome (mm10) using TopHat with default settings (Kim et al., 2013). We used Cuff-diff v2 to (1) estimate FPKM values for known transcripts and (2) analyze differentially expressed transcripts. In all differential expression tests, a difference was considered significant if the q value was <0.05 (Cuff-diff default). A heatmap of gene expression was generated using R language (version 3.2.1) and was generated on the basis of $\log_2$ (FPKM). Gene ontology analysis of gene expression changes was performed using Gene Set Enrichment Analysis (GSEA; https://www.broadinstitute.org/gsea/index.jsp).

ChIP-qPCR

ChIP-qPCR assays were performed as previously described (Wang et al., 2020). Control and Si*Brg1* (5′-CUGCUAAAUACAAACUCAA[dT][dT]-3′)-treated Oli-neu cells were fixed by 1% formaldehyde to crosslink DNA with endogenous proteins, and chromatin was prepared from shearing with a Covaris S220 sonicator. H3K27me3 antibody (active motif, 61018) or control immunoglobulins (immunoglobulin G [IgG]) in the presence of protein A/G Sepharose CL-4B beads was used for immunoprecipitation overnight at 4°C. After reverse crosslink, proteinase K treatment, the precipitated chromatin DNA was purified for PCR. Primers were designed on the promoter regions, and the amount of DNA was quantified by qPCR. The fold enrichment of H3K27me3 was calculated over IgG. PCR primer sequences are listed in Table S2.

Western blotting

Control and Si*Brg1*(5′-CUGCUAAAUACAAACUCAA[dT][dT]-3′)-treated Oli-neu cells were lysed in radioimmunoprecipitation assay buffer containing protease and phosphatase inhibitors. The cell lysis was then centrifuged at 15,000 × *g*. for 20 min at 4°C. After the determination of protein concentration (Bio-Rad), the supernatants were heated in reducing SDS sample buffer at 95°C for 15 min and then separated by 8–12% SDS-PAGE. The separated proteins were transferred to 0.45 μM membrane (Millipore) and then blocked by 5% non-fat milk in T-PBS buffer for 1 h at room temperature. Followed by washing in T-PBS three times, the membrane was then incubated with the primary antibodies at 4°C overnight. The antibodies used were rabbit anti-BRG1 (sc-10768; Santa Cruz Biotechnology, RRID: AB_2255022), rabbit anti-EED (17-10034; Millipore, RRID: AB_10615775), rabbit anti-H3k27me3 (9733; Cell Signaling Technology, RRID: AB_2616029), rabbit anti-EZH2 (5246; Cell Signaling Technology, RRID: AB_10694683), and rabbit anti-SUZ12 (13701; Cell Signaling Technology, RRID: AB_2798295). Mouse anti-GAPDH (MAB374; Millipore, RRID: AB_2107445) was used as an input control. The membrane was then washed with T-PBS three times and incubated with secondary antibodies conjugated to horseradish peroxidase (Jackson ImmunoResearch Laboratories) in 5% milk in T-PBS for 1 h at room temperature. After washing three times, the bands were visualized with ECL Western blotting detection reagents (Pierce) per the manufacturer's instructions and quantified by ImageJ software.

Coimmunoprecipitation analysis

For exogenous coimmunoprecipitation (Co-IP), Oli-neu cells were transfected with HA-EED plasmid using Polyjet for 48 h and harvested in a lysis buffer containing protease and phosphatase inhibitors. Cell lysates were centrifuged at 13,000 rpm for 30 min at 4°C and then the supernatants were incubated with 20 μl of magnetic anti-HA beads (B26202; Bimake) overnight at 4°C under rotation. Subsequently, the beads were washed with cold lysis buffer and the immunoprecipitated proteins were analyzed by Western blotting with the ECL kit. The antibodies used were rabbit anti-BRG1 (sc-10768; Santa Cruz Biotechnology, RRID: AB_2255022), mouse anti-GAPDH (MAB374; Millipore, RRID: AB_2107445), and rabbit anti-HA (2367S; Cell Signaling Technology, RRID: AB_10691311). Secondary antibodies conjugated to HRP were from Jackson ImmunoResearch Laboratories.

For endogenous Co-IP: Primary mouse OPCs were cultured and then harvested in a lysis buffer containing protease and phosphatase inhibitors. Cell lysates were centrifuged at 13,000 rpm for 30 min at 4°C and then the supernatants were incubated with 2 μg of IgG or anti-BRG1 antibody and immunoprecipitated using Protein A/G beads (sc-2003; Santa Cruz Biotechnology) overnight at 4°C under rotation. Subsequently, the procedures were performed as described above. The antibodies used were rabbit anti-BRG1 (sc-10768; Santa Cruz Biotechnology, RRID: AB_2255022), rabbit anti-EED (85322; Cell Signaling Technology, RRID: AB_2923355), rabbit anti-H3k27me3 (9733; Cell Signaling Technology, RRID: AB_2616029), and mouse anti-GAPDH (MAB374; Millipore, RRID: AB_2107445). Secondary antibodies conjugated to HRP were from Jackson ImmunoResearch Laboratories.

Luciferase assay

Control and ZIC4 or SP9-overexpressed Oli-neu cells were co-transfected with luciferase reporter *Olig2*-Luc or *Mbp*-Luc, and Renilla-Luc was used as an internal control. Firefly and Renilla luciferase activities were measured sequentially with the Luciferase assay kit (E1910; Promega). Firefly luciferase activity was normalized to Renilla luciferase activity.

Quantification and statistics

All analyses were done using GraphPad Prism 8.00 (https://www.graphpad.com). All data are shown as mean ± SEM. Data distribution was assumed to be normal, but this was not formally tested. Statistical significance was determined using two-tailed Student's *t* tests or two-way ANOVA with Sidak's multiple comparisons test. Significance was set as * for $P < 0.05$, ** for $P < 0.01$, and ***$P < 0.001$ unless otherwise indicated. Quantifications were performed from at least three independent experiments. No randomization was used to collect all the data but they were quantified blindly.

Online supplemental material

Fig. S1 shows astrocytes and microglia are not affected in the *Brg1* iKO-*Pdgfra* brain. Fig. S2 shows that *Brg1* deletion in CNP$^+$ immature OLs causes a developmental delay in OL differentiation. Table S1 shows a differentially expressed gene list in Fig. 4 C. Table S2 shows the primer list used in Figs. 4, 6, and 7.

Data availability

All data are present in the paper and/or the online supplemental material and will be made available upon request. RNA-seq data have been deposited in the NCBI Gene Expression Omnibus (GEO) under accession number GEO: GSE205236. SUZ12 ChIP-seq data was from GEO: GSE82211. RNA-seq data of Eed KO OPC was from GEO: GSE135880.

Acknowledgments

The authors thank Sean Ogurek for technical assistance, X. Zhou for cartoon drawing, and Dr. Klaus Nave for the *Cnp*-Cre line.

Jiajia Wang performed experiments at the Cincinnati Children's Hospital and her current affiliation is Zhejiang University. She is supported by the National Natural Science Foundation of China (no. 82104181). Q.R. Lu was in part supported by the National Multiple Sclerosis Society award (RG2110).

Author contributions: Jiajia Wang and Q.R. Lu conceptualized the study; Jiajia Wang, L. Yang, Y. Du, X. Liu, and E. Nicholson performed experiments and analyzed data; Jiajia Wang, L. Yang, Jincheng Wang, and X. Liu performed RNA-seq, ChIP-seq, and data analysis; Q.R. Lu, M. Xin and Q. Weng provided resources and inputs. J. Wang and Q.R. Lu wrote and edited the manuscript with inputs from all authors. Q.R. Lu supervised the project.

Disclosures: The authors declare no competing interests exist.

Submitted: 30 October 2023
Revised: 1 March 2024
Accepted: 28 March 2024

References

Alexander, J.M., S.K. Hota, D. He, S. Thomas, L. Ho, L.A. Pennacchio, and B.G. Bruneau. 2015. Brg1 modulates enhancer activation in mesoderm lineage commitment. *Development*. 142:1418–1430. https://doi.org/10.1242/dev.109496

Azim, K., and A.M. Butt. 2011. GSK3β negatively regulates oligodendrocyte differentiation and myelination in vivo. *Glia*. 59:540–553. https://doi.org/10.1002/glia.21122

Bercury, K.K., and W.B. Macklin. 2015. Dynamics and mechanisms of CNS myelination. *Dev. Cell*. 32:447–458. https://doi.org/10.1016/j.devcel.2015.01.016

Bergles, D.E., and W.D. Richardson. 2015. Oligodendrocyte development and plasticity. *Cold Spring Harb. Perspect. Biol.* 8:a020453. https://doi.org/10.1101/cshperspect.a020453

Berry, K., J. Wang, and Q.R. Lu. 2020. Epigenetic regulation of oligodendrocyte myelination in developmental disorders and neurodegenerative diseases. *F1000 Res.* 9:F1000 Faculty Rev-105. https://doi.org/10.12688/f1000research.20904.1

Berry, K.P., and Q.R. Lu. 2020. Chromatin modification and epigenetic control in functional nerve regeneration. *Semin. Cell Dev. Biol.* 97:74–83. https://doi.org/10.1016/j.semcdb.2019.07.009

Bischof, M., M. Weider, M. Küspert, K.A. Nave, and M. Wegner. 2015. Brg1-dependent chromatin remodelling is not essentially required during oligodendroglial differentiation. *J. Neurosci.* 35:21–35. https://doi.org/10.1523/JNEUROSCI.1468-14.2015

Centore, R.C., G.J. Sandoval, L.M.M. Soares, C. Kadoch, and H.M. Chan. 2020. Mammalian SWI/SNF chromatin remodeling complexes: Emerging mechanisms and therapeutic strategies. *Trends Genet.* 36:936–950. https://doi.org/10.1016/j.tig.2020.07.011

Elsen, G.E., L.Y. Choi, K.J. Millen, Y. Grinblat, and V.E. Prince. 2008. Zic1 and Zic4 regulate zebrafish roof plate specification and hindbrain ventricle morphogenesis. *Dev. Biol.* 314:376–392. https://doi.org/10.1016/j.ydbio.2007.12.006

Emery, B., and J.C. Dugas. 2013. Purification of oligodendrocyte lineage cells from mouse cortices by immunopanning. *Cold Spring Harb. Protoc.* 2013:854–868. https://doi.org/10.1101/pdb.prot073973

Emery, B., and Q.R. Lu. 2015. Transcriptional and epigenetic regulation of oligodendrocyte development and myelination in the central nervous system. *Cold Spring Harb. Perspect. Biol.* 7:a020461. https://doi.org/10.1101/cshperspect.a020461

Fletcher, R.B., D. Das, L. Gadye, K.N. Street, A. Baudhuin, A. Wagner, M.B. Cole, Q. Flores, Y.G. Choi, N. Yosef, et al. 2017. Deconstructing olfactory stem cell trajectories at single-cell resolution. *Cell Stem Cell*. 20:817–830.e8. https://doi.org/10.1016/j.stem.2017.04.003

Floriddia, E.M., T. Lourenço, S. Zhang, D. van Bruggen, M.M. Hilscher, P. Kukanja, J.P. Gonçalves Dos Santos, M. Altınkök, C. Yokota, E. Llorens-Bobadilla, et al. 2020. Distinct oligodendrocyte populations have spatial preference and different responses to spinal cord injury. *Nat. Commun.* 11:5860. https://doi.org/10.1038/s41467-020-19453-x

Franklin, R.J., and S.A. Goldman. 2015. Glia disease and repair-remyelination. *Cold Spring Harb. Perspect. Biol.* 7:a020594. https://doi.org/10.1101/cshperspect.a020594

Hargreaves, D.C., and G.R. Crabtree. 2011. ATP-Dependent chromatin remodeling: Genetics, genomics and mechanisms. *Cell Res.* 21:396–420. https://doi.org/10.1038/cr.2011.32

Ho, L., and G.R. Crabtree. 2010. Chromatin remodelling during development. *Nature*. 463:474–484. https://doi.org/10.1038/nature08911

Ho, L., E.L. Miller, J.L. Ronan, W.Q. Ho, R. Jothi, and G.R. Crabtree. 2011. esBAF facilitates pluripotency by conditioning the genome for LIF/STAT3 signalling and by regulating polycomb function. *Nat. Cell Biol.* 13:903–913. https://doi.org/10.1038/ncb2285

Hota, S.K., and B.G. Bruneau. 2016. ATP-dependent chromatin remodeling during mammalian development. *Development*. 143:2882–2897. https://doi.org/10.1242/dev.128892

Kessaris, N., M. Fogarty, P. Iannarelli, M. Grist, M. Wegner, and W.D. Richardson. 2006. Competing waves of oligodendrocytes in the forebrain and postnatal elimination of an embryonic lineage. *Nat. Neurosci.* 9:173–179. https://doi.org/10.1038/nn1620

Khandker, L., M.A. Jeffries, Y.J. Chang, M.L. Mather, A.V. Evangelou, J.N. Bourne, A.K. Tafreshi, I.M. Ornelas, O. Bozdagi-Gunal, W.B. Macklin, and T.L. Wood. 2022. Cholesterol biosynthesis defines oligodendrocyte precursor heterogeneity between brain and spinal cord. *Cell Rep.* 38:110423. https://doi.org/10.1016/j.celrep.2022.110423

Kim, D., G. Pertea, C. Trapnell, H. Pimentel, R. Kelley, and S. Salzberg. 2013. TopHat2: accurate alignment of transcriptomes in the presence of insertions, deletions and gene fusions. *Genome Biol.* 14:R36. https://doi.org/10.1186/gb-2013-14-4-r36

Koreman, E., X. Sun, and Q.R. Lu. 2018. Chromatin remodeling and epigenetic regulation of oligodendrocyte myelination and myelin repair. *Mol. Cell. Neurosci.* 87:18–26. https://doi.org/10.1016/j.mcn.2017.11.010

Li, D., R.C. Ahrens-Nicklas, J. Baker, V. Bhambhani, A. Calhoun, J.S. Cohen, M.A. Deardorff, A. Fernández-Jaén, B. Kamien, M. Jain, et al. 2020. The variability of SMARCA4-related Coffin-Siris syndrome: Do nonsense candidate variants add to milder phenotypes? *Am. J. Med. Genet. A.* 182:2058–2067. https://doi.org/10.1002/ajmg.a.61732

Li, J., C. Wang, Z. Zhang, Y. Wen, L. An, Q. Liang, Z. Xu, S. Wei, W. Li, T. Guo, et al. 2018. Transcription factors Sp8 and Sp9 coordinately regulate olfactory bulb interneuron development. *Cereb. Cortex*. 28:3278–3294. https://doi.org/10.1093/cercor/bhx199

Li, J., Y. Xi, W. Li, R.L. McCarthy, S.A. Stratton, W. Zou, W. Li, S.Y. Dent, A.K. Jain, and M.C. Barton. 2017. TRIM28 interacts with EZH2 and SWI/SNF to activate genes that promote mammosphere formation. *Oncogene*. 36:2991–3001. https://doi.org/10.1038/onc.2016.453

Li, N., M. Kong, S. Zeng, C. Hao, M. Li, L. Li, Z. Xu, M. Zhu, and Y. Xu. 2019. Brahma related gene 1 (Brg1) contributes to liver regeneration by epigenetically activating the Wnt/β-catenin pathway in mice. *FASEB J.* 33:327–338. https://doi.org/10.1096/fj.201800197R

Liu, N., C.L. Peterson, and J.J. Hayes. 2011. SWI/SNF- and RSC-catalyzed nucleosome mobilization requires internal DNA loop translocation within nucleosomes. *Mol. Cell. Biol.* 31:4165–4175. https://doi.org/10.1128/MCB.05605-11

Matsumoto, S., F. Banine, K. Feistel, S. Foster, R. Xing, J. Struve, and L.S. Sherman. 2016. Brg1 directly regulates Olig2 transcription and is required for oligodendrocyte progenitor cell specification. *Dev. Biol.* 413:173–187. https://doi.org/10.1016/j.ydbio.2016.04.003

Matsumoto, S., F. Banine, J. Struve, R. Xing, C. Adams, Y. Liu, D. Metzger, P. Chambon, M.S. Rao, and L.S. Sherman. 2006. Brg1 is required for murine neural stem cell maintenance and gliogenesis. *Dev. Biol.* 289:372–383. https://doi.org/10.1016/j.ydbio.2005.10.044

McKenzie, I.A., D. Ohayon, H. Li, J.P. de Faria, B. Emery, K. Tohyama, and W.D. Richardson. 2014. Motor skill learning requires active central myelination. *Science*. 346:318–322. https://doi.org/10.1126/science.1254960

Menon, D.U., Y. Shibata, W. Mu, and T. Magnuson. 2019. Mammalian SWI/SNF collaborates with a polycomb-associated protein to regulate male germline transcription in the mouse. *Development*. 146:dev174094. https://doi.org/10.1242/dev.174094

Nishiyama, A., T. Shimizu, A. Sherafat, and W.D. Richardson. 2021. Life-long oligodendrocyte development and plasticity. *Semin. Cell Dev. Biol.* 116:25–37. https://doi.org/10.1016/j.semcdb.2021.02.004

O'Rourke, M., C.L. Cullen, L. Auderset, K.A. Pitman, D. Achatz, R. Gasperini, and K.M. Young. 2016. Evaluating tissue-specific recombination in a Pdgfr alpha-CreER(T2) transgenic mouse line. *Plos One*. 11:e0162858. https://doi.org/10.1371/journal.pone.0162858

Runge, J.S., J.R. Raab, and T. Magnuson. 2016. Epigenetic regulation by ATP-dependent chromatin-remodeling enzymes: SNF-Ing out crosstalk. *Curr. Top. Dev. Biol.* 117:1–13. https://doi.org/10.1016/bs.ctdb.2015.10.009

Samanta, J., and J.A. Kessler. 2004. Interactions between ID and OLIG proteins mediate the inhibitory effects of BMP4 on oligodendroglial differentiation. *Development*. 131:4131–4142. https://doi.org/10.1242/dev.01273

Seeker, L.A., N. Bestard-Cuche, S. Jäkel, N.L. Kazakou, S.M.K. Bøstrand, L.J. Wagstaff, J. Cholewa-Waclaw, A.M. Kilpatrick, D. Van Bruggen, M. Kabbe, et al. 2023. Brain matters: Unveiling the distinct contributions of region, age, and sex to glia diversity and CNS function. *Acta Neuropathol. Commun.* 11:84. https://doi.org/10.1186/s40478-023-01568-z

Söhl, G., S. Hombach, J. Degen, and B. Odermatt. 2013. The oligodendroglial precursor cell line Oli-neu represents a cell culture system to examine functional expression of the mouse gap junction gene connexin29 (Cx29). *Front. Pharmacol.* 4:83. https://doi.org/10.3389/fphar.2013.00083

Sokpor, G., Y. Xie, J. Rosenbusch, and T. Tuoc. 2017. Chromatin remodeling BAF (SWI/SNF) complexes in neural development and disorders. *Front. Mol. Neurosci.* 10:243. https://doi.org/10.3389/fnmol.2017.00243

Sun, L.O., S.B. Mulinyawe, H.Y. Collins, A. Ibrahim, Q. Li, D.J. Simon, M. Tessier-Lavigne, and B.A. Barres. 2018. Spatiotemporal control of CNS myelination by oligodendrocyte programmed cell death through the TFEB-PUMA Axis. *Cell*. 175:1811–1826.e1821. https://doi.org/10.1016/j.cell.2018.10.044

Tolstorukov, M.Y., C.G. Sansam, P. Lu, E.C. Koellhoffer, K.C. Helming, B.H. Alver, E.J. Tillman, J.A. Evans, B.G. Wilson, P.J. Park, and C.W. Roberts. 2013. Swi/Snf chromatin remodeling/tumor suppressor complex establishes nucleosome occupancy at target promoters. *Proc. Natl. Acad. Sci. USA*. 110:10165–10170. https://doi.org/10.1073/pnas.1302209110

Tsurusaki, Y., N. Okamoto, H. Ohashi, T. Kosho, Y. Imai, Y. Hibi-Ko, T. Kaname, K. Naritomi, H. Kawame, K. Wakui, et al. 2012. Mutations affecting components of the SWI/SNF complex cause Coffin-Siris syndrome. *Nat. Genet.* 44:376–378. https://doi.org/10.1038/ng.2219

Vasko, A., T.G. Drivas, and S.A. Schrier Vergano. 2021. Genotype-phenotype correlations in 208 individuals with Coffin-Siris syndrome. *Genes*. 12:12. https://doi.org/10.3390/genes12060937

Wang, J., L. Yang, C. Dong, J. Wang, L. Xu, Y. Qiu, Q. Weng, C. Zhao, M. Xin, and Q.R. Lu. 2020. EED-mediated histone methylation is critical for CNS myelination and remyelination by inhibiting WNT, BMP, and senescence pathways. *Sci. Adv.* 6:eaaz6477. https://doi.org/10.1126/sciadv.aaz6477

Weber, C.M., A. Hafner, J.G. Kirkland, S.M.G. Braun, B.Z. Stanton, A.N. Boettiger, and G.R. Crabtree. 2021. mSWI/SNF promotes polycomb repression both directly and through genome-wide redistribution. *Nat. Struct. Mol. Biol.* 28:501–511. https://doi.org/10.1038/s41594-021-00604-7

Wegner, M. 2008. A matter of identity: Transcriptional control in oligodendrocytes. *J. Mol. Neurosci.* 35:3–12. https://doi.org/10.1007/s12031-007-9008-8

Weng, Q., J. Wang, J. Wang, D. He, Z. Cheng, F. Zhang, R. Verma, L. Xu, X. Dong, Y. Liao, et al. 2019. Single-cell transcriptomics uncovers glial progenitor diversity and cell fate determinants during development and gliomagenesis. *Cell Stem Cell*. 24:707–723.e8. https://doi.org/10.1016/j.stem.2019.03.006

Xiao, C., L. Gao, Y. Hou, C. Xu, N. Chang, F. Wang, K. Hu, A. He, Y. Luo, J. Wang, et al. 2016. Chromatin-remodelling factor Brg1 regulates myocardial proliferation and regeneration in zebrafish. *Nat. Commun.* 7:13787. https://doi.org/10.1038/ncomms13787

Xiong, Y., W. Li, C. Shang, R.M. Chen, P. Han, J. Yang, K. Stankunas, B. Wu, M. Pan, B. Zhou, et al. 2013. Brg1 governs a positive feedback circuit in the hair follicle for tissue regeneration and repair. *Dev. Cell*. 25:169–181. https://doi.org/10.1016/j.devcel.2013.03.015

Yu, J.R., C.H. Lee, O. Oksuz, J.M. Stafford, and D. Reinberg. 2019. PRC2 is high maintenance. *Genes Dev*. 33:903–935. https://doi.org/10.1101/gad.325050.119

Yu, Y., Y. Chen, B. Kim, H. Wang, C. Zhao, X. He, L. Liu, W. Liu, L.M. Wu, M. Mao, et al. 2013. Olig2 targets chromatin remodelers to enhancers to initiate oligodendrocyte differentiation. *Cell*. 152:248–261. https://doi.org/10.1016/j.cell.2012.12.006

Yue, T., K. Xian, E. Hurlock, M. Xin, S.G. Kernie, L.F. Parada, and Q.R. Lu. 2006. A critical role for dorsal progenitors in cortical myelination. *J. Neurosci.* 26:1275–1280. https://doi.org/10.1523/JNEUROSCI.4717-05.2006

Zarate, Y.A., E. Bhoj, J. Kaylor, D. Li, Y. Tsurusaki, N. Miyake, N. Matsumoto, S. Phadke, L. Escobar, A. Irani, et al. 2016. SMARCE1, a rare cause of Coffin-Siris syndrome: Clinical description of three additional cases. *Am. J. Med. Genet. A.* 170:1967–1973. https://doi.org/10.1002/ajmg.a.37722

Zuchero, J.B., and B.A. Barres. 2013. Intrinsic and extrinsic control of oligodendrocyte development. *Curr. Opin. Neurobiol.* 23:914–920. https://doi.org/10.1016/j.conb.2013.06.005

Supplemental material

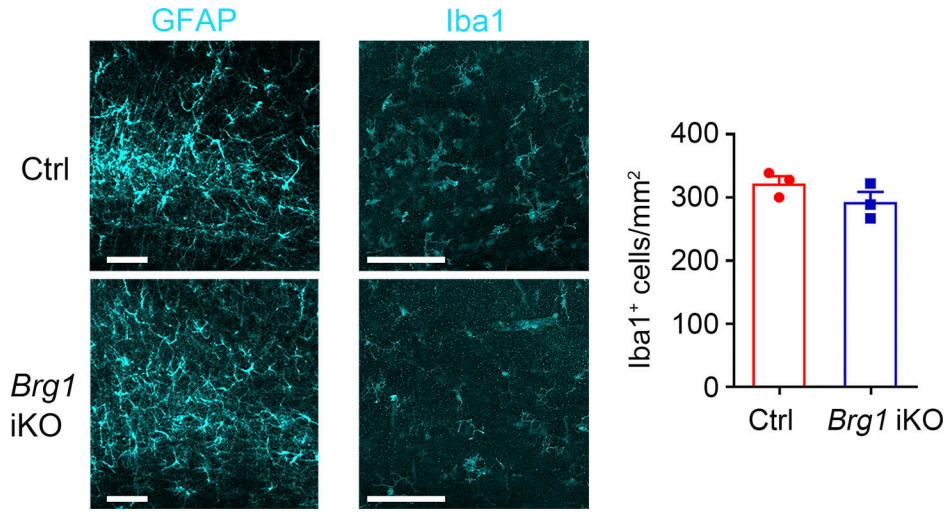

Figure S1. **Astrocytes and microglia are not affected in the *Brg1* iKO-*Pdgfra* brain.** Immunostaining of GFAP and Iba1 in the brain of control and Brg1 iKO-*Pdgfra* mice at P7 (left). Quantification of Iba1⁺ cells in the corpus callosum from P7 control and Brg1 iKO-*Pdgfra* mice (right). Data are presented as mean ± SEM; $n = 3$ animals/genotype; two-tailed unpaired Student's t test.

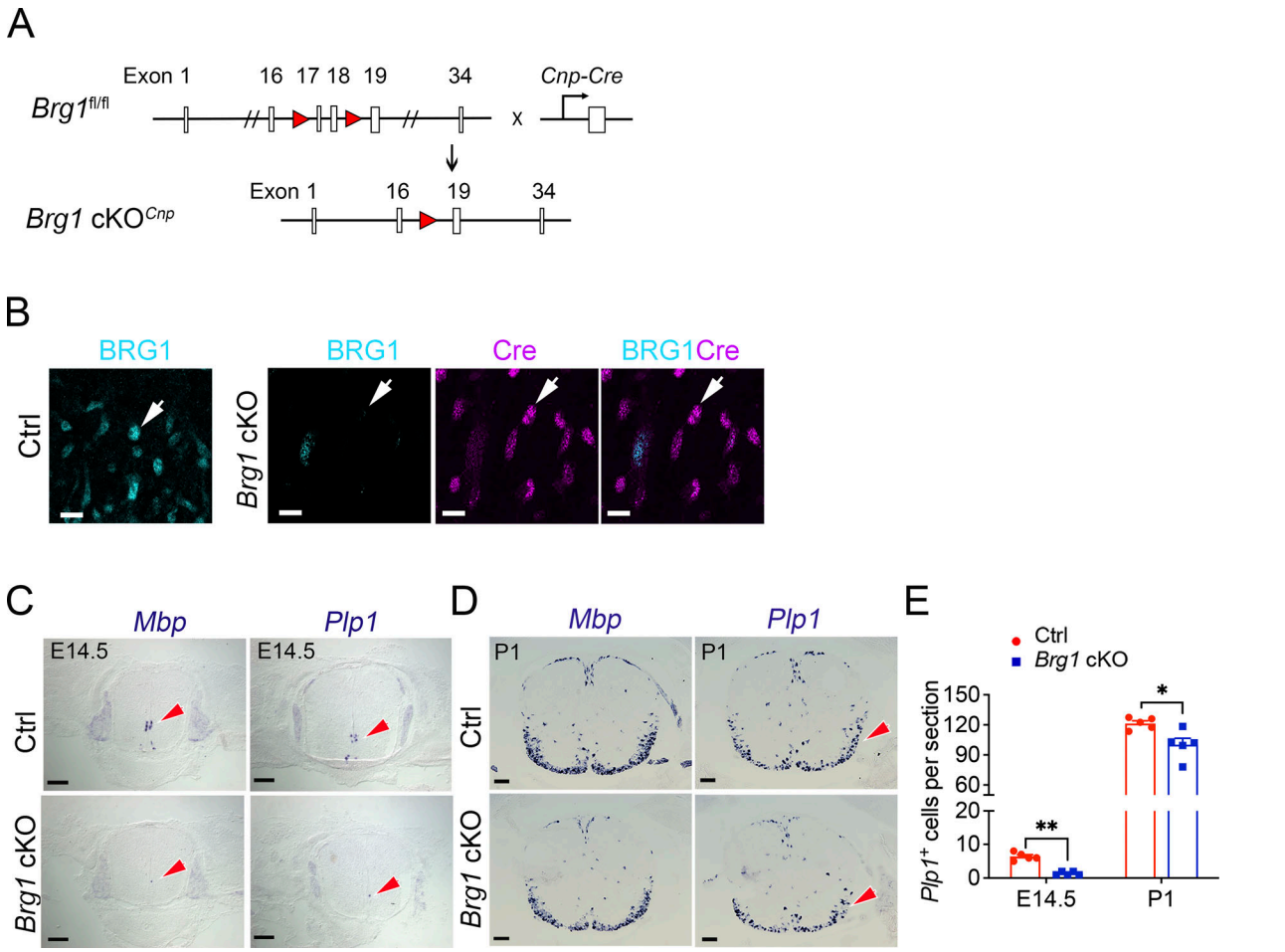

Figure S2. ***Brg1* deletion in *Cnp*⁺ immature OLs causes a developmental delay in OL differentiation. (A)** Strategy used to conditional delete *Brg1* by *Cnp-Cre* mice. **(B)** Representative immunostaining of BRG1 and Cre in the white matter of control (*Brg1*$^{fl/fl}$ and *Brg1* cKO-*Cnp* spinal cord at P1. Arrow (left), BRG1⁺ cell; arrow (right), Cre⁺ cell. Scale bar, 10 µm; *n* = 3 animals/genotype. **(C and D)** In situ hybridization for *Mbp* and *Plp1* on spinal cord sections of control and *Brg1* cKO-*Cnp* mice at E14.5 (C) and P1 (D). Scale bar, 100 µm; *n* = 5 animals/genotype. **(E)** Quantification of *Plp1*⁺ cell number in one section. *n* = 5 animals/genotype. Data are presented as mean ± SEM; *P < 0.05; **P < 0.01; two-tailed unpaired Student's *t* test (E).

Provided online are Table S1 and Table S2. Table S1 shows the differentially expressed gene list in Fig. 4 C. Table S2 lists primers used in this study.